

New Constraints on Deformation, Slip Rate, and Timing of the Most Recent Earthquake on the West Tahoe–Dollar Point Fault, Lake Tahoe Basin, California

by Daniel S. Brothers, Graham M. Kent, Neal W. Driscoll, Shane B. Smith, Robert Karlin, Jeffrey A. Dingler, Alistair J. Harding, Gordon G. Seitz, and Jeffrey M. Babcock

Abstract High-resolution seismic compressed high intensity Radar pulse (CHIRP) data and piston cores acquired in Fallen Leaf Lake (FLL) and Lake Tahoe provide new paleoseismic constraints on the West Tahoe–Dollar Point fault (WTDPF), the westernmost normal fault in the Lake Tahoe Basin, California. Paleearthquake records along three sections of the WTDPF are investigated to determine the magnitude and recency of coseismic slip. CHIRP profiles image vertically offset and folded strata along the southern and central sections that record deformation associated with the most recent event (MRE) on the WTDPF. Three faults are imaged beneath FLL, and the maximum vertical offset observed across the primary trace of the WTDPF is ~ 3.7 m. Coregistered piston cores in FLL recovered sediment and organic material above and below the MRE horizon. Radiocarbon dating of organic material constrained the age of the MRE to be between 3.6 and 4.9 k.y. B.P., with a preferred age of 4.1–4.5 k.y. B.P. In Lake Tahoe near Rubicon Point, approximately 2.0 m of vertical offset is observed across the WTDPF. Based on nearby core data, the timing of this offset occurred between ~ 3 –10 k.y. B.P., which is consistent with the MRE age in FLL. Offset of Tioga-aged glacial deposits provides a long-term record of vertical deformation on the WTDPF since ~ 13 –14 k.y. B.P., yielding a slip rate of 0.4–0.8 mm/yr. In summary, the slip rate and earthquake potential along the WTDPF is comparable to the nearby Genoa fault, making it the most active and potentially hazardous fault in the Lake Tahoe Basin.

Introduction

The Lake Tahoe Basin (LTB) is one of several fault-controlled basins within the northern Walker Lane deformation belt (Unruh *et al.*, 2003). Based on westward dipping lake deposits and the structural tilt of the Carson Range, the LTB appears to be an asymmetric half-graben (Hyne *et al.*, 1972; Schweickert *et al.*, 1999; Surpless *et al.*, 2002; Dingler, 2007) separating the Sierra Nevada Range to the west from the Carson Range to the east (Fig. 1). Extension occurs along three primary normal fault systems: the West Tahoe–Dollar Point fault (WTDPF), the Stateline–North Tahoe fault (SLNTF), and the Incline Village fault (IVF). Each fault exhibits down-to-the-east normal displacement during the last 10 k.y. (Dingler, 2007). Until recently, geologic slip rates, earthquake timing, and magnitude estimates across faults in the LTB were poorly constrained. Offshore swath bathymetry and compressed high intensity Radar pulse (CHIRP) sub-bottom surveys combined with cores and onshore paleoseismic excavations have defined the regional distribution of faults and the first precise estimates on slip rates (Gardner

et al., 2000; Kent *et al.*, 2005; Dingler, 2007). Despite such advances, one of the most active, but poorly understood, structures is the north–south striking WTDPF (Fig. 1). Along strike fault morphology (Fig. 1), large cumulative displacement beneath Lake Tahoe and vertically offset Pleistocene glacial moraines in the southern LTB indicate the WTDPF has a relatively high slip rate. Nevertheless, relaxed scarp profiles measured south of Lake Tahoe suggest the fault has not experienced a ground-rupturing event for several thousand years.

In 2006, we acquired CHIRP sub-bottom data and piston cores along the southern section of the WTDPF between Emerald Bay and Christmas Valley to define the age, coseismic offset, and rupture length of the most recent event (MRE; Fig. 2). High-resolution marine geophysics provides an opportunity not only to identify offset strata associated with individual earthquakes, but also to define the regional fault architecture in an area that is inaccessible by traditional onshore methods. Our results, combined with previous sub-

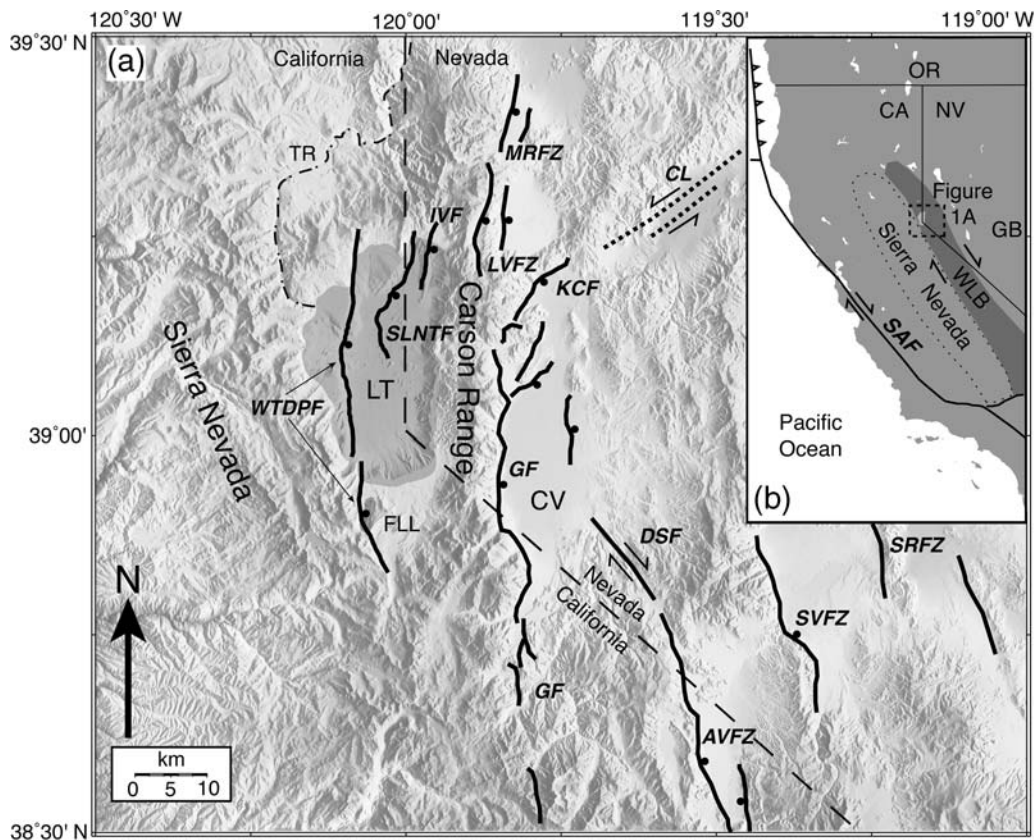


Figure 1. (a) Generalized fault and shaded relief map of eastern California and western Nevada. The LTB lies between the Sierra Nevada and Carson Ranges. Lake Tahoe (LT) and FLL are shaded gray. Solid black lines are active fault systems; dashed black lines are inferred faults. Abbreviations: West Tahoe–Dollar Point fault, WTDPF; Stateline–North Tahoe fault, SLNTF; Incline Village fault, IVF; Genoa fault, GF; Mount Rose fault zone, MRFZ; Little Valley fault zone, LVFZ; Carson Lineament, CL; Kings Canyon fault, KCF; Deep Springs fault, DSF; Antelope Valley fault zone, AVFZ; Smith Valley fault, SVF; Smith Range fault zone, SRFZ; Truckee River, TR; and Carson Valley CV. (b) Simplified plate boundary highlighting the San Andreas fault (SAF), Walker Lane belt (WLB; shaded gray area), Sierra Nevada block (thin dashed line), and the Great Basin (GB).

bottom and piston core data collected in Lake Tahoe (Dingler, 2007), indicate the WTDPF is the most active and hazardous fault in the LTB. The relatively high slip rate and rupture potential of the WTDPF provides essential information for geohazards assessments, including probability estimates for a future, large-magnitude event.

Quaternary Geology and Tectonics

Walker Lane

The Walker Lane belt (WLB) is an actively deforming tectonic province situated between the relatively stable Sierra Nevada microplate on the west and the central Great Basin to the east (Stewart, 1988; Argus and Gordon, 2001). The WLB is a complex zone of dextral transtension responding to the oblique-divergent motion of the Sierra Nevada microplate relative to the central Great Basin (Fig. 1b; Bennett *et al.*, 2003; Oldow, 2003; Unruh *et al.*, 2003). A suite of geodetic studies have detected 9–13 mm/yr of mostly dextral shear partitioned across numerous strike-slip, dip-slip, and

oblique-slip faults in the Walker Lane, accounting for ~25% of the total plate motion between the North American and Pacific plates (Hearn and Humphreys, 1998; Dixon *et al.*, 2000; Svarc *et al.*, 2002; Bennett *et al.*, 2003; Hammond and Thatcher, 2004, 2007).

Lake Tahoe is within the northern WLB, which consists of a series of north–south trending, normal fault bounded mountain ranges, northwest striking dextral faults, and northeast striking sinistral faults (Faulds *et al.*, 2005). At the latitude of Lake Tahoe and east of the Sierra Nevada Range the topography is dominated by several uplifted mountain ranges (Wassuk, Singatse, Pine Nut, and Carson) that are bounded by north–south striking normal faults. Although Surpluss *et al.* (2002) document larger cumulative offset along normal fault systems to the east than those to the west, geodetic studies indicate that the majority of extension (between 2–3 mm/yr) is focused around the Sierra Nevada frontal fault system. Near Lake Tahoe, the Sierra Nevada frontal fault system splays into two extensional domains separated by the Carson Range: the LTB and Carson Valley (Unruh *et al.*, 2003). Measured geodetic rates across the LTB

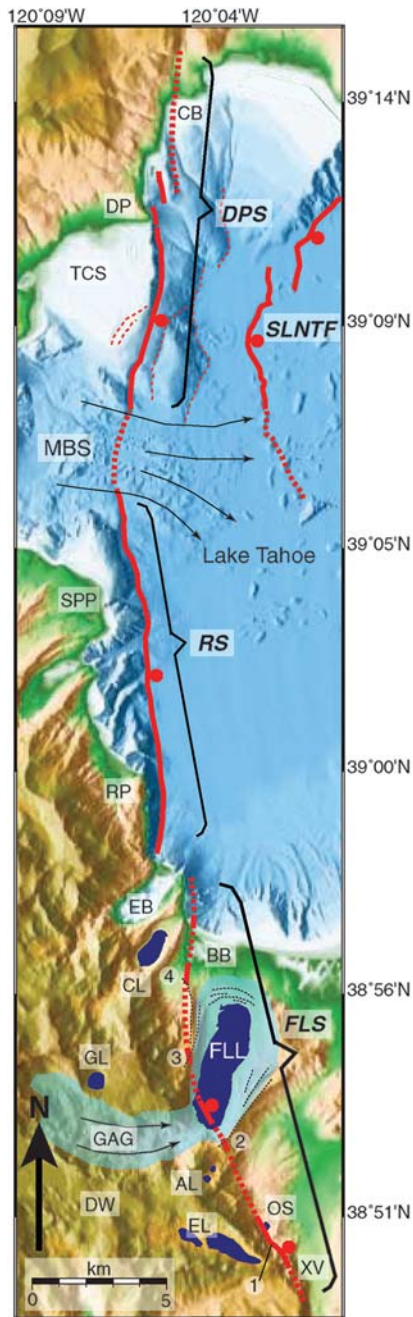


Figure 2. Map showing the three sections of the WTDPF (solid red lines—where known, and dashed red lines—where inferred): Dollar Point section (DPS), Rubicon section (RS), and Fallen Leaf section (FLS). Thin dashed red lines surrounding the DPS represent slump scarps. Abbreviations: Christmas Valley, XV; Osgood Swamp, OS; Echo Lakes, EL; Desolation Wilderness, DW; Angora Lakes, AL; Glenn Alpine glacier (also where the present Glen Alpine Creek is sourced), GAG; Gilmore Lake, GL; Cascade Lake, CL; Baldwin Beach, BB; Emerald Bay, EB; Rubicon Point, RP; Sugar Pine Point, SPP; McKinney Bay slide, MBS; Tahoe City shelf, TCS; Dollar Point, DP; and Carnelian Bay, CB. Black arrows represent flow directions for the MBS and GAG (also shaded blue). Dashed black lines surrounding FLL are approximate locations of moraine crests; arcuate crests north of FLL are recessional moiraines. Numbered features: (1) photographed scarp in Figure 14, (2) and (3) 2–3 m scarps offsetting Tioga-aged moraine crests on either side of FLL, and (4) 2–3 m meadow scarp.

are poorly resolved due to sparse coverage on the western side of the Basin. Results of geologic and geodetic studies in the region, point to a westward encroachment of extension from the western Basin and Range province into the eastern Sierra Nevada block (Henry and Perkins, 2001; Surpless *et al.*, 2002). The present day Sierra Nevada–WLB boundary is located along the WTDPF. North of the LTB, Global Positioning System (GPS) studies measured ~ 7 mm/yr of dextral shear across the northern WLB, representing $\sim 15\%$ of the total plate motion (Bennett *et al.*, 2003; Hammond and Thatcher, 2004, 2007). Paleoseismic studies in the northern WLB have uncovered evidence for large-magnitude Holocene ruptures along normal, dextral, and sinistral fault systems, including the IVF (Dingler, 2007), Genoa fault (GF; Ramelli *et al.*, 1999), Pyramid Lake fault (Briggs and Wesnousky, 2004), and the Olinghouse fault (Briggs and Wesnousky, 2005).

Lake Tahoe Basin

The LTB has been tectonically active since at least 3 Ma (Henry and Perkins, 2001; Surpless *et al.*, 2002; Faulds *et al.*, 2005) with extension occurring along a series of east-dipping normal faults. The Quaternary landscape has been shaped by several Wisconsin glacial advances between 79 and 15 k.y. B.P. (Bischoff and Cummins, 2001), forming several moraine-bounded valleys along the range fronts within the LTB. The Sierra Nevada and Carson Ranges are predominantly composed of granodiorite and related metamorphic roof pendants of the Sierra Nevada batholith (Saucedo *et al.*, 2005), but also Miocene and younger volcanic rocks are found in the northern LTB (Birkeland, 1963; Saucedo *et al.*, 2005). Seismic reflection data collected in Lake Tahoe have imaged up to ~ 300 m of sediment below the lake floor without reaching the acoustic basement (AB, Hyne *et al.*, 1972).

The basin exhibits abundant low-magnitude seismicity (Ichinose *et al.*, 1999, 2003; Smith *et al.*, 2004). New paleoseismic evidence suggests there have been large-magnitude Holocene events (Kent *et al.*, 2005; Dingler, 2007). Late-Pleistocene to present geologic slip-rate estimates were calculated based on offset geomorphic markers observed in sub-bottom CHIRP profiles (Kent *et al.*, 2005; Dingler, 2007). An offset 19.2 ± 1.8 ka wave-cut paleoterrace, which correlates temporally with a 19 ± 1 ka glacial advance during the Tioga glaciation (Phillips *et al.*, 1996), was used to calculate a minimum basin extension rate of ~ 0.5 mm/yr (Kent *et al.*, 2005). In addition to offshore studies, an excavation across the IVF revealed the first direct evidence for multiple $M \approx 7$ Holocene events in the LTB (Dingler, 2007).

West Tahoe–Dollar Point Fault. The WTDPF is the north–south striking, range bounding normal fault along the western margin of the LTB (Figs. 1 and 2). Most of the fault's length is located beneath Lake Tahoe where, presumably, the cumulative throw is greatest. Swath bathymetry and sub-bottom CHIRP surveys reveal well-defined scarps through

debris aprons, slides, and lake bottom sediments (Hyne *et al.*, 1972; Gardner *et al.*, 2000; Kent *et al.*, 2005; Dingler, 2007). We divide the WTDPF into three sections that are defined by apparent discontinuities or geomorphic boundaries (Fig. 2). The Fallen Leaf section extends from Christmas Valley at the south through Fallen Leaf Lake (FLL) and offshore into Lake Tahoe at the western edge of Baldwin Beach. Prior to this study, the Fallen Leaf section was poorly understood. Fault scarps within the transition between the Fallen Leaf and Rubicon sections are not well expressed by the local morphology and may include more than one splay. After an apparent ~1 km northwestward step from below Eagle Point to the base of the submerged slope off Emerald Point, the Rubicon section continues northward to McKinney Bay. Although the trends of the two northern sections are nearly equivalent and evidence for a tectonic boundary has not been observed, we treat the McKinney Bay slide (MBS) as a section boundary because faulting beneath the slide is poorly imaged and scarps have been overprinted or eroded by debris aprons and/or landslides. The southern extent of the Dollar Point section begins at the northern edge of the MBS and continues to the north along the eastern edge of the Tahoe City shelf (TCS) then eventually steps onshore in the vicinity of Carnelian Bay. A series of scarps and offset strata below the TCS appear to be caused by slumping (Dingler, 2007). The total length of the WTDPF is greater than 50 km.

Fallen Leaf Lake. FLL, located ~2 km south of Baldwin Beach, provides another lacustrine environment in which the WTDPF can be imaged using marine seismic methods. FLL is ~45 m higher than Lake Tahoe and fills a narrow moraine-bounded glacial valley (Fig. 2). The overall morphology has been shaped by Pleistocene glaciers sourced in the Desolation Wilderness (Fig. 2) where Tahoe-aged glaciers seem to have been more significant than the more recent Tioga-aged glaciers that merely reworked the inner slopes of Tahoe moraines (Saucedo *et al.*, 2005). The entire valley is bounded on either side by > 300 m high-lateral moraines (measured from the lake floor) that extend towards Lake Tahoe for > 5 km from the range front. Near its northern shoreline, FLL is bounded by a series of Tioga-aged recessional and terminal moraines that separate it from Lake Tahoe (Saucedo *et al.*, 2005). Based on the dimensions of lateral and end moraines, the Tahoe and Tioga glaciers in Fallen Leaf Valley appear to have been much larger than the adjacent valley glaciers that occupied Cascade Lake and Emerald Bay. Sediment discharge from Glen Alpine Creek, the most significant modern sediment input to FLL, would have been strongly modulated by glacial melt water. Like much of the LTB, glacial morphology, fluvial incision, and dense vegetation surrounding FLL make onshore identification of fault scarps difficult. Offshore geophysical surveys offer an alternative method to study the interactions between tectonic and glacial or fluvial processes.

Methods

Detailed geophysical surveys and field reconnaissance mapping were conducted between Christmas Valley and Emerald Bay in July 2006 (Figs. 2 and 3). Two sub-bottom surveys conducted in FLL and offshore Baldwin Beach in Lake Tahoe employed the Scripps Institution of Oceanography's Edgetech CHIRP profiler. In FLL, the CHIRP profiler was mounted on an aluminum frame held afloat by two inflatable pontoons and towed by a small (~20 × 10 ft) platform barge operated by the Fallen Leaf Marina. More than 40 line-km of data were collected at a constant tow depth of ~1 m. Offshore Baldwin Beach the CHIRP was towed off the stern of the R/V LeConte (operated by University of California, Davis) at 2–3 m below the surface; over 12 line-km of data were collected. All data were digitally recorded in SEG-Y format with real-time GPS navigation recorded with each shot, providing absolute location accuracy to within 5 m. SEG-Y files were processed using SIOSEIS then imported into the Kingdom Suite and Fledermaus software packages for interpretation. The 1–6 kHz swept frequency acoustic source provided sub-bottom penetration to > 50 m in lacustrine sediments, but in some places penetration was limited by the AB. All depth conversions assumed a 1500 m/sec sediment velocity unless otherwise stated. Onshore field reconnaissance between Baldwin Beach and Christmas Valley identified scarps along the Fallen Leaf lateral moraines as well as a several kilometer-long scarp south of FLL near Osgood Swamp (Fig. 2). The onshore and offshore results were integrated with datasets collected in 2000, 2002, and 2006 along the Rubicon and Dollar Point sections of the WTDPF (Kent *et al.*, 2005; Dingler, 2007).

During October 2006, five piston cores were collected in FLL (Figs. 3 and 4) from a platform barge using a modified Kullenberg piston corer. The coring device includes an ~250 kg weight stand, a 5 m long, 3 inch diameter core barrel and, depending on the sediment type, typically recovers between 3 and 5 m of sediment. The cores were acquired in the southern half of FLL in the vicinity of the WTDPF in an effort to construct a chronostratigraphic framework that can be used to estimate the timing of the MRE. Each of the piston cores recovered > 3.5 m of sediment. Lithologic and magnetic susceptibility logs were produced for all cores. The stratigraphy in all cores except one, PC5, was easily correlated based on color, texture, lithology, and magnetic susceptibility patterns (Fig. 4). Increases in magnetic susceptibility generally reflect increased concentrations of magnetite-rich siliciclastic sediments and may be correlated with periods of increased sediment contribution from the basin margins or in this case from Glen Alpine Creek. Conversely, low magnetic susceptibility appears to correlate with increased amounts of nonmagnetic clays and silts. PC5 was located at a shallower depth along the eastern basin slope. Six detrital wood samples and one organic fiber sample extracted from cores PC3, PC4, and PC5 were radiocarbon dated using an accelerator mass spectrometer. PC5 was the

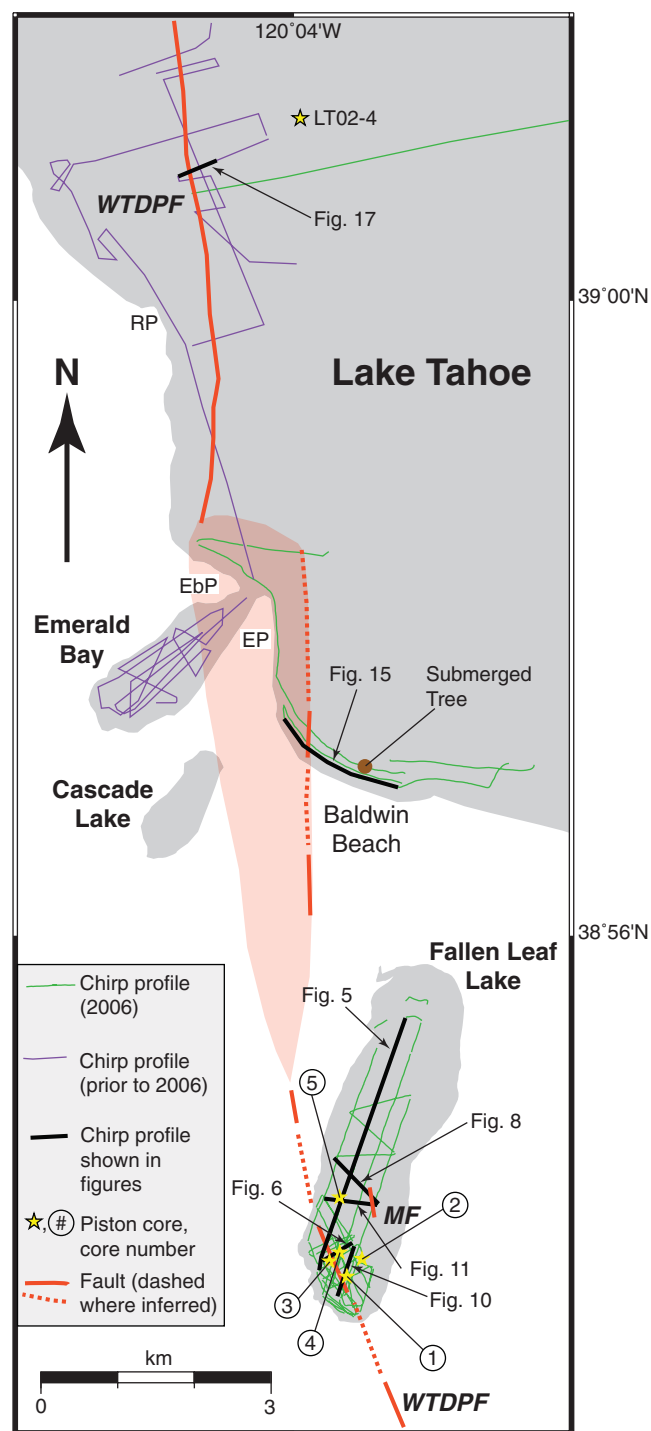


Figure 3. CHIRP profiles and sediment core locations in FLL and southwestern Lake Tahoe. Red lines mark the location of the WTDPF and MF (solid red line—where known, and dashed red line—where inferred). Abbreviations: RP, Rubicon Point; Eagle Point, EP; and Emerald Point, EmP. The submerged tree (brown circle) was sampled and radiocarbon dated to test for coincident timing of its submersion and the MRE on the WTDPF (Table 1). LT02-4 is the location of a piston core used to constrain sedimentation rates near the Rubicon section of the WTDPF shown in Figure 17 (Smith *et al.*, 2007). The precise location of faulting between FLL and EmP is not clear and may be distributed across a complex relay zone (red shaded area).

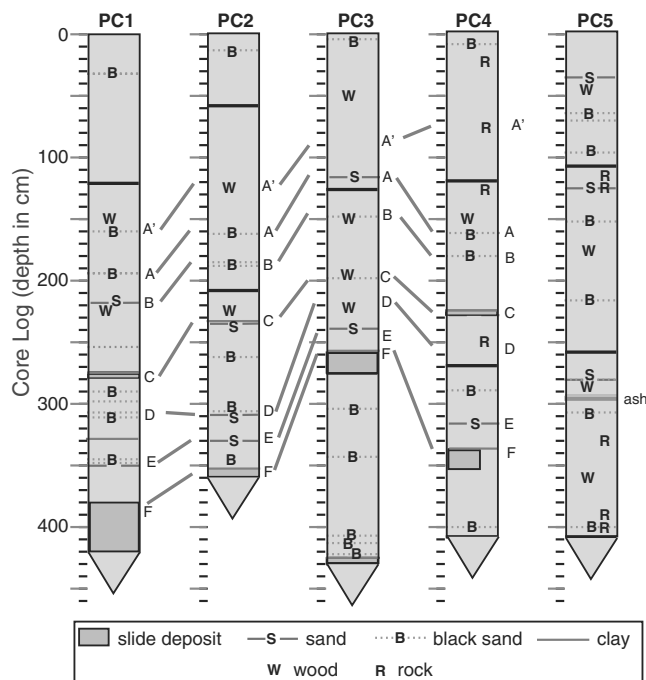


Figure 4. Piston core logs. Stratigraphic correlations are based on color, lithology, and magnetic susceptibility. Note the distinct slide deposit that is recognized in four of the cores. The ash labeled in PC5 is the 7.6–8.0 k.y. B.P. Tsoyowata Ash (Bacon, 1983).

only core that contained the 7.5–8.0 k.y. old Tsoyowata Ash as a chronological marker bed (Bacon, 1983; Sarna-Wojkicki *et al.*, 1991). Once the chronostratigraphy was established based on core data, we correlated distinct marker beds in the cores with corresponding layers in the seismic stratigraphy, allowing us to constrain the age of tectonically offset seismic horizons.

Faulting and Stratigraphic Framework

Fallen Leaf Lake

A high-density grid of sub-bottom CHIRP profiles was collected in the southern portion of the lake surrounding the WTDPF and a less dense grid collected in the northern lake (Fig. 3). The survey afforded three-dimensional, basin-wide correlation between seismic horizons and a nearly complete characterization of recent tectonic, glacial, and sedimentary processes beneath FLL. A low-resolution bathymetric elevation model was constructed by gridding lake-floor elevations measured in the CHIRP profiles. The basin depocenter is in the southern lake and is bounded to the south by a steep, ~100 m high escarpment that trends obliquely to the long axis of the valley and glacial flow direction. The base of the slope and its trend are coincident with the WTDPF, which is delineated by vertically offset and folded lacustrine horizons. In general, horizontally layered lacustrine deposits infill topographic relief in the underlying AB (Fig. 5). Three faults beneath FLL are observed in the CHIRP profiles. Two parallel faults separated by ~80 m trend ~N25°W along

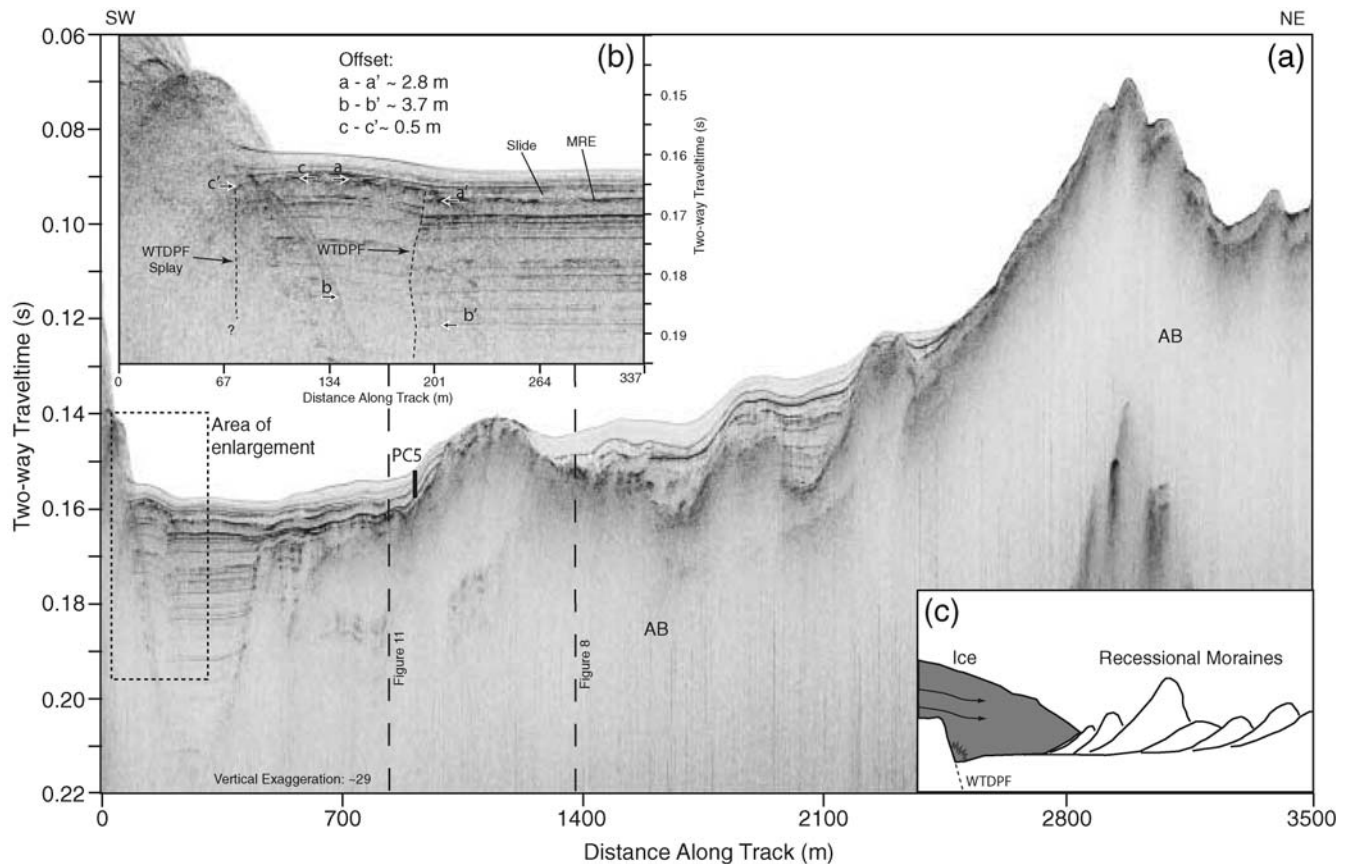


Figure 5. (a) Northeast–southwest trending CHIRP profile spanning over two-thirds of FLL. The WTDPF is seen toward the southern end, adjacent to a steep, fault-parallel escarpment. (b) Enlarged section of the two splays of the WTDPF (dashed box in 5a). Offset across both faults creates anticlinal folding in the sediments. A divergent bed labeled “slide” thickens into the fault and infills accommodation created during the MRE. The slide is an important marker bed that is seen in the seismic stratigraphy and in four of the piston cores (Fig. 4) throughout most of the southern lake. Piercing points (white arrows) on the footwall were selected near the apex of the anticline; beds are assumed to have been deposited approximately horizontal, then were subsequently folded and offset during the MRE. Offset increases with depth from ~ 2.8 m across the MRE horizon (aa') to ~ 3.7 m across horizon bb' due to increased compaction and dewatering with depth (all travel time to depth conversions assume 1500 m/sec velocity). Piston core PC5 is ~ 40 m to the west of this profile. (c) Hummocky topography in the acoustic basement (AB) is seen in several profiles. This type of morphology is typical for moraines formed at glacier fronts by temporary still stands or readvancements during an overall glacial retreat. Similar morphology is observed as a series of arcuate recessional moraines between FLL and Lake Tahoe (Saucedo, 2005). The relief toward the southern end of the profile, adjacent to the WTDPF, may be formed by a combination of glacial and tectonic processes, much like a roche moutonnée, but glacial plucking may have been facilitated by the location of the fault.

the base of the steep escarpment in the southern lake and project onto scarps mapped on the moraine crests above FLL (Fig. 2). Based on their proximity and synthetic nature, the two faults are collectively referred to as the WTDPF. The third fault, termed the Midlake fault (MF), is located ~ 1 km to the northeast of the WTDPF (Fig. 3) and is observed in only two profiles.

Coseismic deformations in the shallow sub-bottom are identified as vertically folded strata, but down-section layers show greater separation and exhibit distinct offset, suggesting that extensional fault-propagation-folding has occurred (Gawthorpe *et al.*, 1997; Hardy and McClay, 1999). East-side-down folding (~ 5 m below the lake floor) demarcates the MRE horizon on both the WTDPF and MF (Figs. 6–8). The MRE horizon on the hanging wall dips into the fault and is overlain by a thin divergent layer that thickens toward

the fault reflecting syntectonic deposition and infill of the accommodation created during the MRE. A striking observation is that the MRE horizon and the thin divergent bed overlying the MRE horizon can be traced across both the WTDPF and the MF (Fig. 9). Throughout the southern half of the lake the divergent layer onlaps bathymetric highs and diverges and thickens into lows, ranging in thickness from 0– ~ 1.5 m. Near the southeastern slope, strata beneath the layer abruptly changes in character, where it becomes chaotic and appears to have been disrupted (Fig. 10). Based on acoustic character and core logs (discussed later), we refer to this layer as a slide deposit. The stratal geometry and acoustic character seen in Figures 8 and 11 provide a stratigraphic framework that is used for basin-wide interpretations. The smooth lenticular shaped units labeled A, B, and C in package I thicken away from the bathymetric lows and down lap

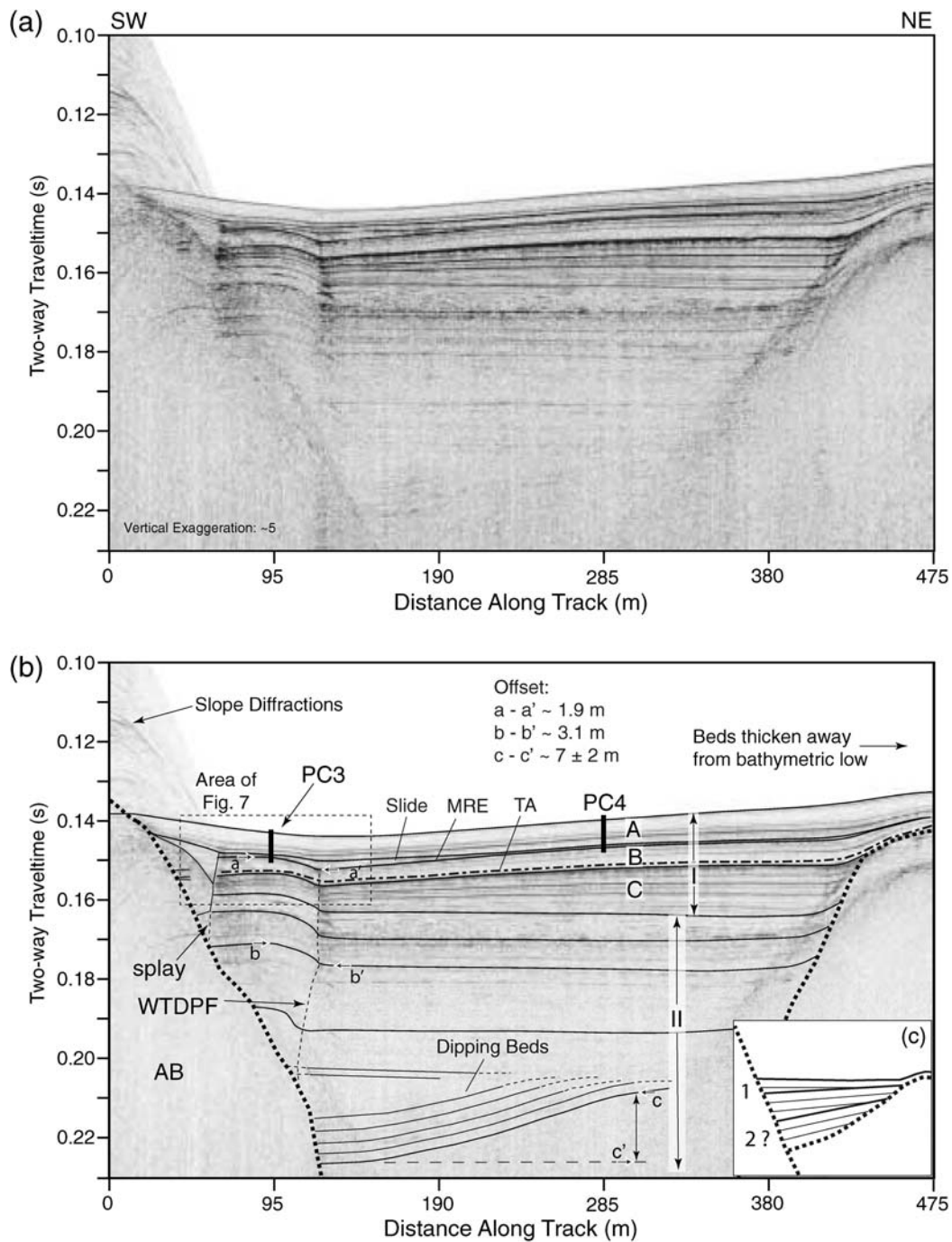


Figure 6. (a) Uninterpreted, and (b) interpreted fault-perpendicular profile. Locations of two nearby cores are projected onto the cross section. Piercing points (white arrows) measure slip that occurred during the MRE. Although offset of the MRE horizon is ~ 1.9 m then increases to ~ 3.1 m over deeper horizons, we do not observe stratigraphic evidence for multiple events (e.g., increase in dip or divergence down section) in the upper ~ 35 m. The deformation resembles a normal fault propagation fold, where offset at depth is attenuated in the shallow, unconsolidated sediments and is expressed as a fold. A slide deposit directly above the MRE horizon infills accommodation created during the MRE. Piston core PC3 sampled the slide near the WTDPF, which is used as a marker bed throughout the lake. Radiocarbon samples from PC3 constrain the timing of the MRE to 4.1–4.5 k.y. B.P. (Table 1). Units A, B and C in section I represent fine-grained layers (low amplitude reflections) that are separated by thin, coarse-grained layers (high-amplitude reflections). The fine-grained layers appear to thicken away from the basin depocenter suggesting current-controlled deposition (see text). The approximate position of the Tsoyowata Ash (dashed line labeled TA; ~ 7 m depth adjacent to the WTDPF) is correlated from seismic sections near piston core PC5 and provides an independent constraint on sedimentation rate. Section II exhibits more uniform deposition. Faintly imaged strata in the hanging wall dip at $\sim 4^\circ$. Assuming the beds were deposited horizontally then subsequently tilted during a penultimate event, the vertical offset is estimated at 7 ± 2 m. (c) Conceptual model for syntectonic deposition, where divergent beds record subsidence along the fault and multiple events can be recognized by increased dip down section.

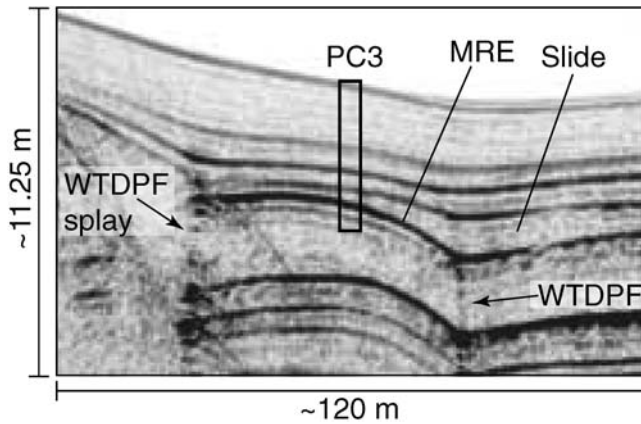


Figure 7. Enlarged section (dashed box) from Figure 6 highlighting the MRE horizon and overlying slide deposit. The two faults are separated by ~ 60 m. Piston core PC3 sampled material above and below the MRE horizon.

onto underlying beds. In contrast, the intervening layers diverge and thicken into low points along the basin margins. Package II does not exhibit the same geometric relationships and deposition appears more uniform.

Matching cores with the nearby seismic profiles allowed us to define relationships between seismic stratigraphy and the corresponding lithostratigraphy. Distinct marker beds sampled by the cores were traced onto adjacent CHIRP profiles (Fig. 9). Lithostratigraphy documented in all the piston cores except PC5 includes a distinct coarse-grained slide deposit (Fig. 4). At the base of PC1 is a coarse-grained, massive bed that contained several large pieces of wood and twigs, where PC2, PC3, and PC4 sampled the distal, fine-grained extent of the equivalent layer. The coarse-grained slide deposit observed in the cores correlates well with the divergent bed overlying the MRE horizon seen in the seismic profiles (Figs. 6 and 10). All cores except PC5 are within 30 m of a CHIRP profile; PC5 is within 45 m. The horizontal offset may result in a slight mismatch (< 0.5 m) between seismic stratigraphy and core logs. Another potential source for mismatch is overpenetration (< 0.5 m), which was noted during recovery by mud on the weights above the core barrel.

The age of the MRE was estimated by radiocarbon dating organic material from either side of the MRE horizon. The analysis was based solely on radiocarbon data from core PC3 (Fig. 12), which was located nearest the WTDPF. Sediment recovered by PC3 extended > 1.5 m below the MRE horizon and contained abundant organic matter for radiocarbon dating. Four samples (all > 5 mg) were analyzed with an accelerator mass spectrometer (Table 1). The radiocarbon dates were converted to calendar years B.P. using the OxCal 4.0 radiocarbon calibration software and calibration curve IntCal04.14c (Ramsey, 1995, 2001; Reimer *et al.*, 2004). All further discussions will be in terms of calendar years B.P. The sample at 3.40 m depth was anomalously old for its stratigraphic position suggesting it had a long-residence time in the watershed before deposition in FLL and was excluded

from the analysis. Of the remaining samples, the deepest and oldest (5.3–5.6 k.y. B.P.) was sampled by the core catcher at a depth of ~ 4.3 m, meaning the actual depth is between 4.3 and 4.8 m (accounting for possible overpenetration). Dividing the depth range by the age range resulted in an average sedimentation rate adjacent to the WTDPF between 0.8 and 0.9 mm/yr. An independent comparison can be made using the 7.5–8.0 k.y. B.P. Tsoyowata Ash that was sampled at a depth of 2.95 m in PC5 between two thin sand beds (Fig. 4). The relative stratigraphic position of the ash layer can be projected onto the nearest profile (Fig. 11; ~ 50 m away) and correlated basin wide. The ash is inferred at a depth of 7 ± 2 m adjacent to the WTDPF (labeled TA in Fig. 6), again resulting in an average sedimentation rate of ~ 1 mm/yr.

The age of the MRE horizon is confined by the age of samples 1 and 3 in PC3 (Fig. 13, Table 1). The absolute lower and upper bounds are 3.6 and 4.9 k.y. B.P. based on the radiocarbon ages, but a more precise estimate was calculated by linearly interpolating the age as a function of depth between samples 1 and 3 (Fig. 13). We assume the slide deposit was emplaced rapidly and removed its thickness from the interpolation. The total thickness between samples after removing the slide is 173 cm (the slide is only $\sim 10\%$ of the total thickness between samples) and the MRE horizon is 65 cm below sample 1. Interpolating the age as a function of depth for both the upper and lower age bounds on each sample confines the MRE to 4.1–4.5 k.y. B.P. Uncertainty in this estimate would be introduced by nonlinear sedimentation rates or nonlinear compaction within the interpolation interval during core collection. However, these effects are not quantifiable with the available data, and we do not observe evidence for either.

Piercing points in the seismic stratigraphy are selected to measure vertical offset (white arrows in Figs. 5, 6, and 8). The 1–6 kHz CHIRP source can resolve layers that are vertically separated by greater than ~ 0.4 m. Travel-time intervals between piercing points are measured directly then converted to depth intervals by assuming an interval velocity. We use a nominal velocity (1500 m/sec) for all depth conversions to avoid overestimating the offset measurements, and we incorporate a pick error of ± 0.2 m. At greater depths (> 10 m) where compaction and dewatering are likely, it is possible that seismic velocities reach ~ 1800 m/sec. On the main splay of the WTDPF, deformation within the shallow, poorly consolidated sediments appears to become distributed as folding and possibly minor faulting, which results in an attenuated offset up-section similar to analog models for extensional fault propagation folds (Hardy and McClay, 1999). Offset measurements show a gradual increase in offset with depth from ~ 2 m over the folded MRE horizon to > 3 m across horizons at depths greater than ~ 10 m (Table 2; Figs. 5–7). Because we do not observe any stratigraphic evidence (e.g., divergent beds, increasing dip with depth) for multiple events in the upper 0.05 sec (~ 38 m) of sediment, it is assumed that the deeper measurements provide our best

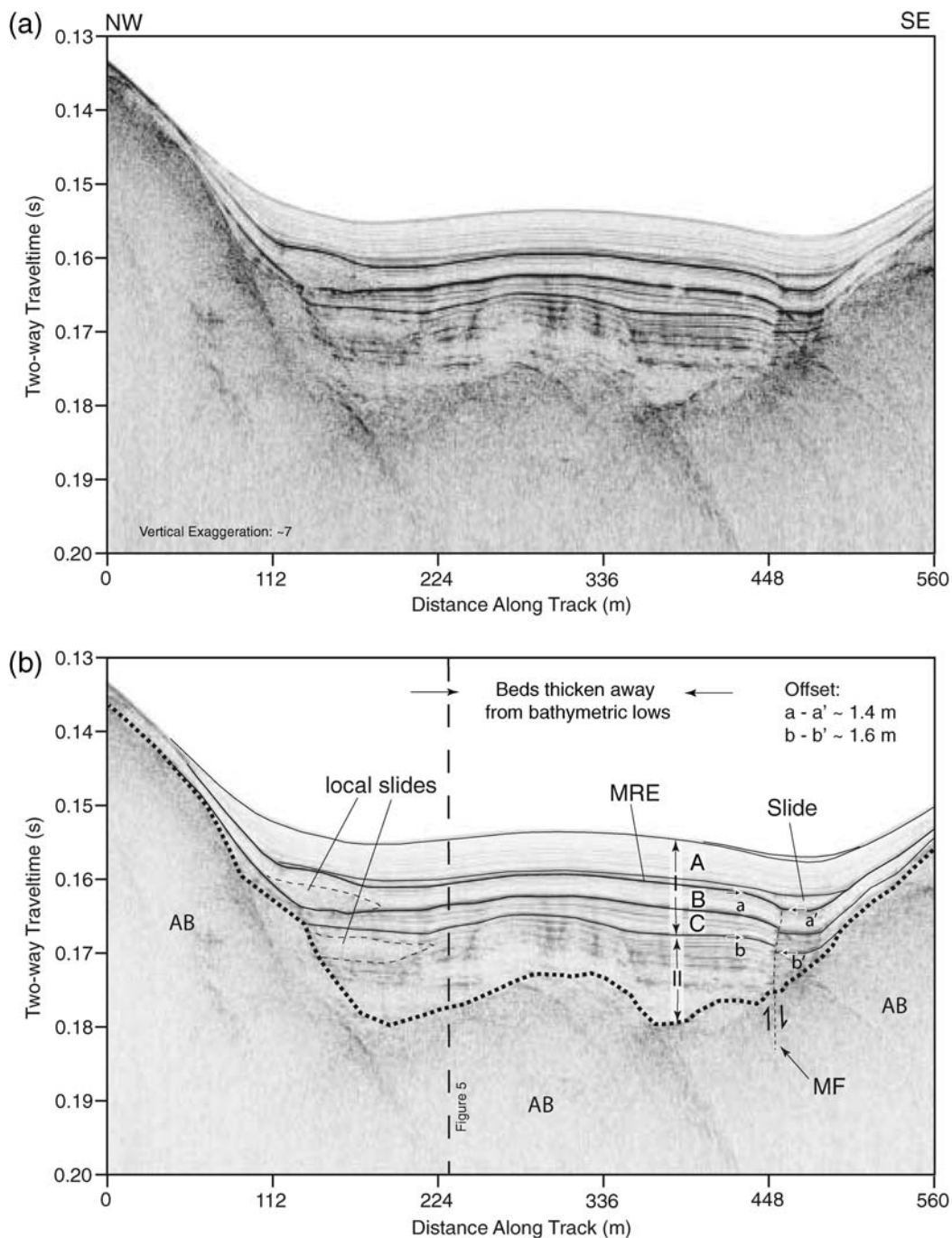


Figure 8. Northeast-southwest oriented profile over the MF and a series of debris slides along the western slope. The MRE horizon and overlying slide are the equivalent layers observed across the WTDPF. Displacement is down-to-the-east and increases from ~ 1.4 m across the MRE horizon to ~ 1.6 m down section. Packages A, B, and C represent lenticular shaped drift deposits (low amplitude) that mantle the underlying topography, but also thicken away from the basin margins. Each unit is separated by thin, coarse-grained gravity slides, one of which is the slide directly above the MRE horizon. Contact surfaces between coarse- and fine-grained deposits result in high-impedance (i.e., high-amplitude) boundaries in the seismic stratigraphy.

estimates for coseismic slip that occurred during the MRE. Overall, nine precise measurements across the MRE horizon ranged between 1.5 and 2.8 m and eight measurements across deeper horizons ranged between 3.0 and 3.7 m (Table 2). The secondary splay (Figs. 5–7), located very near the slope break, is evident in six profiles by small synclinal fold-

ing and infill above the MRE horizon. Offset measurements over the splay ranged from 0.6 to 1.3 m. Although the nature of the splay is poorly imaged, it is possible that the two faults merge at depth and their slip is additive, increasing the total offset produced during the MRE to between 3.6 and 4.5 m, with an average of ~ 4.1 m.

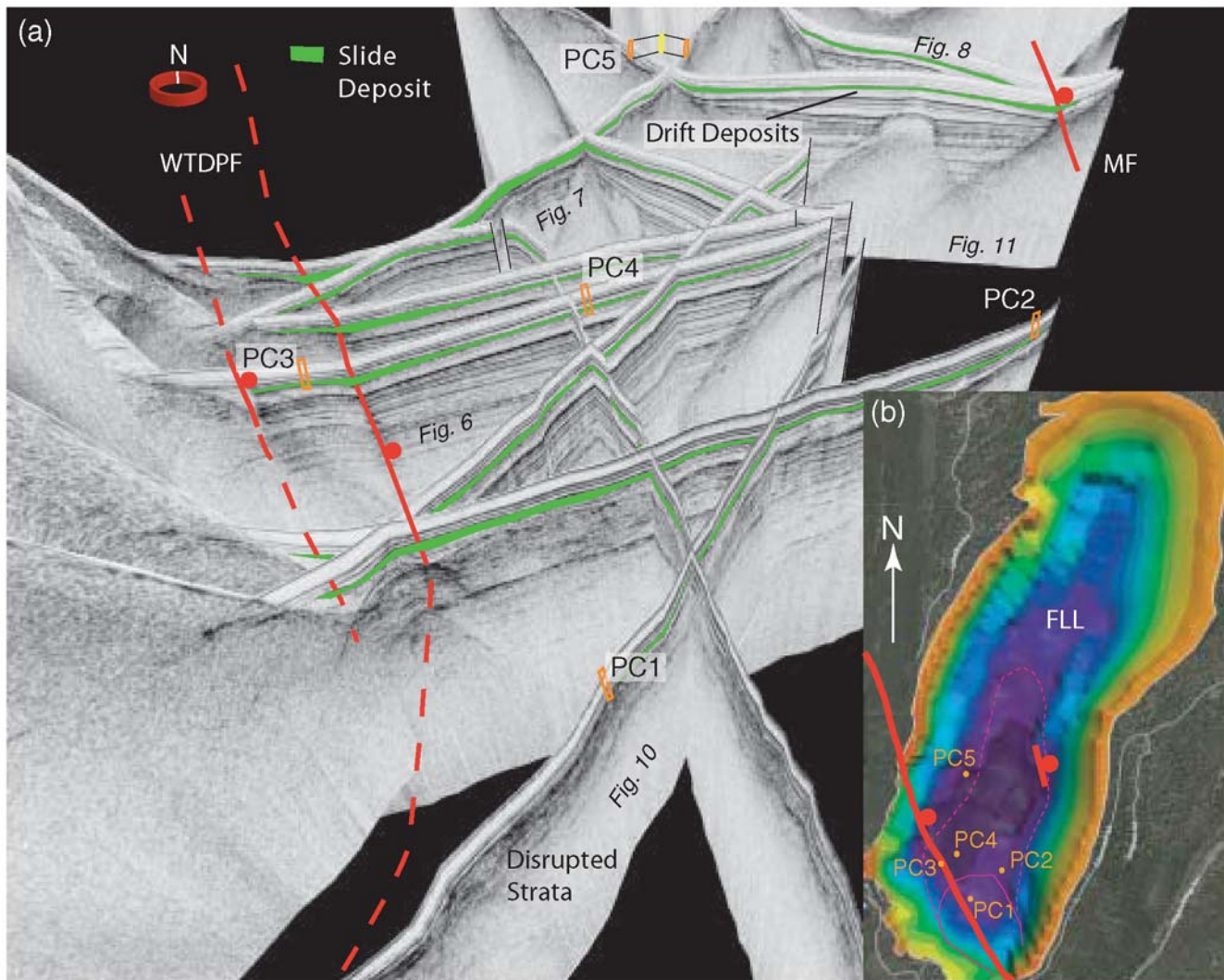


Figure 9. (a) Fence diagram of CHIRP profiles and core locations illustrating the 3-dimensional structure, stratigraphy, and core locations. The diagram illustrates the utility of using acoustic stratigraphy to correlate sediments throughout the basin. PC5 is projected onto the two nearest profiles, but all other cores are within 20 m of the nearest profile. The slide deposit directly above the MRE horizon (green layer) can be traced from its coarse-grained proximal extent to its fine-grained distal reach at the far side of the southern basin. The run-out length is over 1 km. Faults are depicted by red lines (solid red lines, where known and dashed red lines, where inferred). (b) Bathymetric grid of FLL based on CHIRP soundings. Thick red lines are the WTDPF and MF; thin red lines outline the inferred extent of slide deposit (solid red line, proximal and dashed red line, distal).

Approximately 35 m below the lake floor, the stratigraphy abruptly changes in character and has a marked 4° increase in dip toward the fault (Fig. 6). The data quality diminishes down-section due to attenuation and interference from diffractions off the AB and adjacent slopes, but the dipping strata are observed in several profiles and are unlikely to be a three-dimensional artifact or sideswipe from a nearby slope. A dipping horizon that spans the deeper portion of the basin was used as a piercing line and depth was measured at both ends (cc' in Fig. 6). Some ambiguity exists when picking the edges of the horizon resulting in large uncertainty, but the measured difference is $\sim 7 \pm 2$ m (Fig. 5).

The MF is observed in two profiles ~ 1 km northeast of the WTDPF (Figs. 8, 9, and 11). The MRE horizon at the MF

was vertically folded by 1.4 m and is overlain by a divergent wedge similar to that observed across the WTDPF. Offset increases slightly down-section to ~ 1.6 m. The trend of the fault, determined over a length of ~ 100 m, appears parallel to the WTDPF. However, the nearest profile north of the projected trend lacks convincing evidence for faulting. Farther north, disrupted sediments and slide deposits provide weak evidence for a north-south trending fault.

Onshore Mapping

Onshore field reconnaissance mapping south of FLL, near Osgood Swamp (Figs. 2 and 14), revealed a 2.6 km long section of down-to-the-east fault scarps. The scarps offset

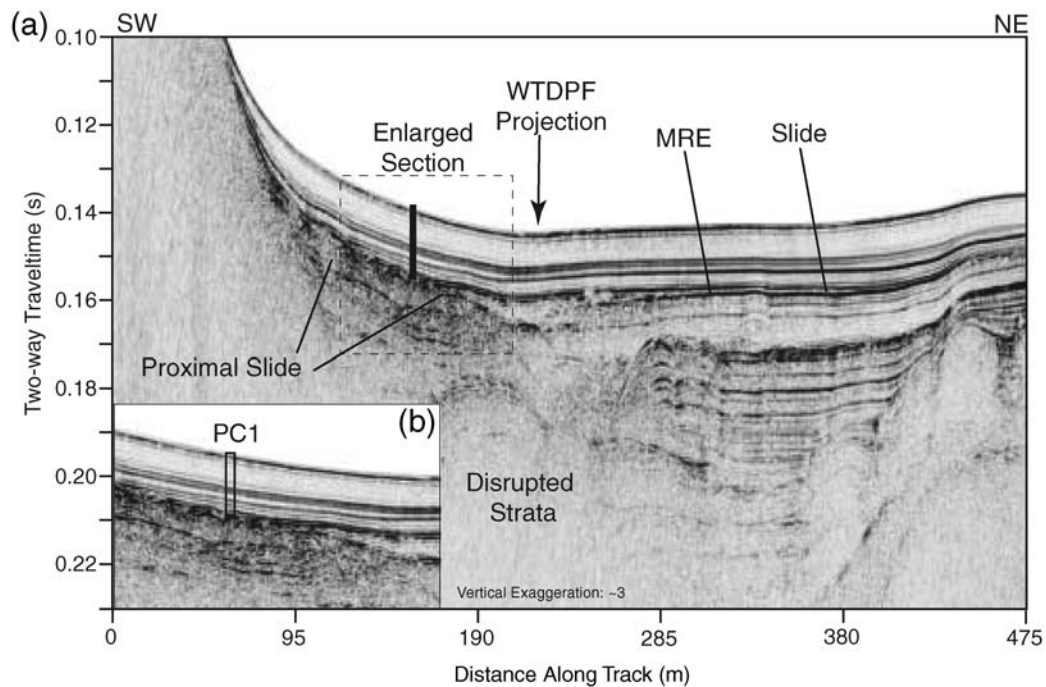


Figure 10. Northeast–southwest oriented type section that confirmed the correlation between the slide material sampled at the base of PC1 (Fig. 4) and highly disrupted, chaotic bedding that grades distally into the divergent bed observed above the MRE horizon.

unconsolidated alluvial and glacial sediments and have relaxed slope profiles. Heights varied depending on the age of the offset material, where some scarps north of Osgood Swamp are 10–15 m high, while others to the south of Osgood Swamp are 2–4 m high (Fig. 14). Between Osgood Swamp and Angora Lakes (Fig. 2) steep slopes and dense vegetation preclude identification of the fault. An ~400 m long, ~3 m high scarp was mapped perpendicular to the Angora Ridge moraine crest (Fig. 2) and aligns with the trend beneath FLL and another ~500 m long scarp mapped on the opposite side of FLL valley. North of FLL, the landscape again becomes covered with dense vegetation and complex fluvial and glacial overprint. A potential ~1 km long scarp was mapped ~2 km south of Baldwin Beach along the edge of a small meadow (Fig. 2). The scarp height in the meadow varies between 3 and 10 m depending on the age of the surface material. Overall, the onshore expression of the WTDPF is poorly constrained, particularly in the region between FLL and Lake Tahoe. Because of the complex geomorphology, subsurface studies are needed to discern fault scarps from glacial or fluvial scarps.

Baldwin Beach

CHIRP data collected along the shallow sandy shelf immediately offshore Baldwin Beach (Fig. 3) show evidence for faulted sediments. A tightly folded syncline (Fig. 15) traced between three profiles and trending north–south aligns with pockmarks and possible lake-floor disruption down the adjacent steep basin slope (Dingler, 2007). The deformation is less obvious than in FLL, possibly due to an absence of

internal bedding in the unconsolidated, medium- to coarse-grained sand.

Several submerged, but rooted trees have been identified near Baldwin Beach and are thought to reflect climatic variability during the mid-Holocene (Lindstrom, 1990). A sample from the deepest submerged tree (Fig. 3), rooted at ~4 m depth and located to the east of the inferred fault (Fig. 3), was radiocarbon dated (Table 1) to test for coincident timing between the MRE on the WTDPF and the tree's inundation. Its age (5.3–5.6 k.y. B.P.; Table 1) is slightly greater than the MRE age range determined at FLL but is consistent with the range of dates determined by Lindstrom (1990).

Rubicon Point to Dollar Point

Several CHIRP profiles discussed by Dingler (2007) were reexamined to define the Rubicon and Dollar Point sections of the WTDPF. Deformation similar to that in FLL is observed across a CHIRP profile at the base of the shelf offshore Rubicon (Figs. 3 and 16). An ~1.4–2.0 m thick section of nearly transparent, unfaulted material overlies a divergent bed that thickens into the fault and infills the small accommodation (Fig. 17). As in FLL, the divergent bed rests directly above the MRE horizon and has a high-amplitude basal reflector suggesting it is a coarse-grained deposit, possibly a gravity slide. The MRE horizon is offset down-to-the-east by 1.0 m (possibly along a synthetic splay of the WTDPF) but farther down-section the offset increases to 2.0 m. Folding is observed ~150 m east of the main fault with horizons offset vertically up to 0.3 m. A piston core located ~800 m from the eastern end of the profile in Figure 3

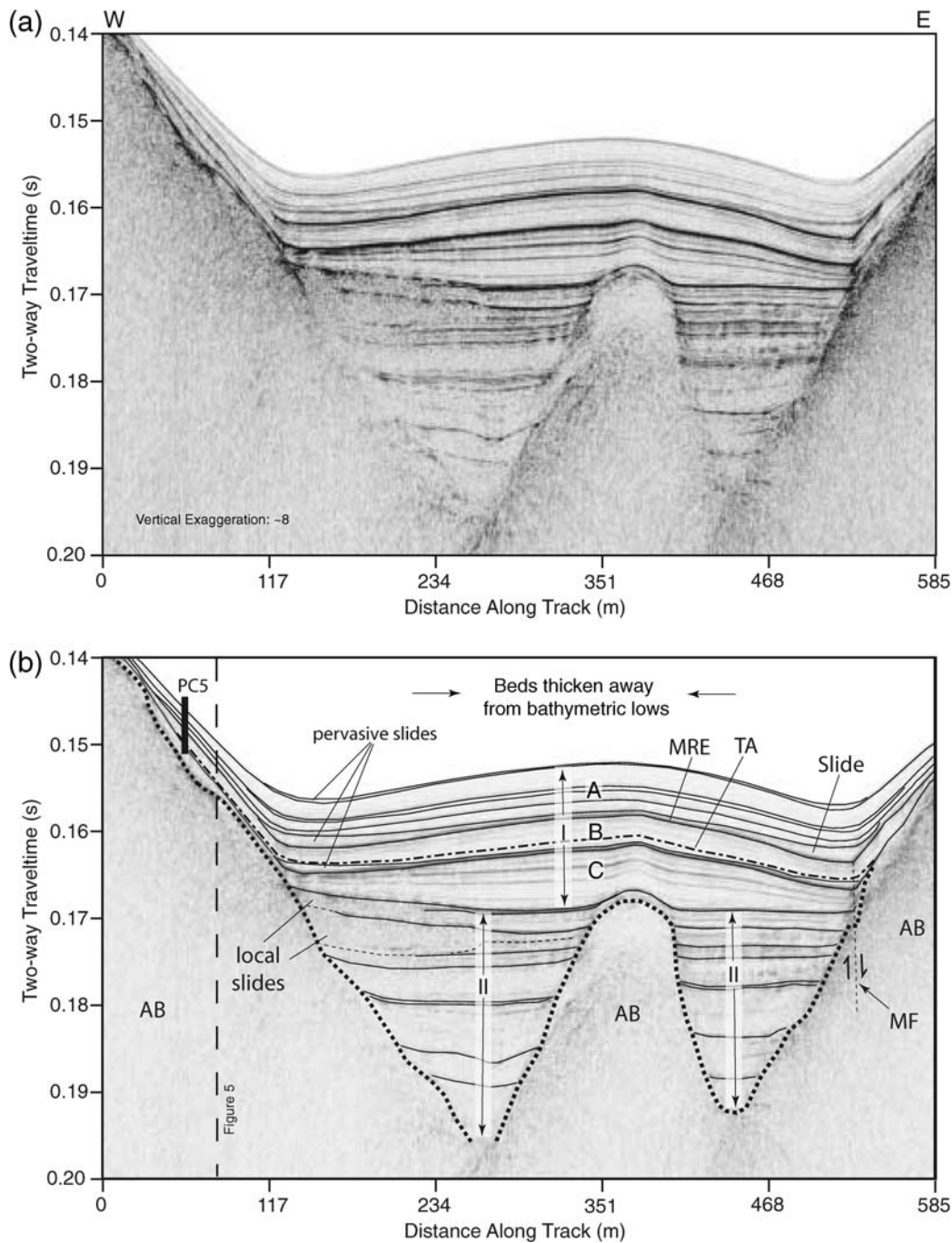


Figure 11. East–west oriented profile highlighting the interplay between current-controlled deposition that forms contourite drifts and down-slope deposits that infill bathymetric low points. Units A, B, and C of section I are separated by coarse-grained slide deposits, resulting in the high-amplitude contacts. The MRE horizon is traced from profiles to the south. Piston core PC5 (~50 m to the north of its projected position shown in the figure) samples the 7.6–8.0 k.y. B.P. Tsoyowata Ash (Fig. 4; Bacon, 1983). The stratigraphic position of the TA is projected onto the seismic section and correlated basin wide. Several thin slides are observed on several profiles, and other local slides are observed to disrupt underlying strata. Evidence for drift deposits is not observed in section II, but small slide complexes are observed along the basin slopes and uniform deposition in topographic lows.

sampled two distinct slide deposits, one at ~0.6 m and the other at ~1.2 m, that have been correlated with several cores to the north and have been dated at 4.1–4.5 k.y. B.P. and 5.3–5.6 k.y. B.P., respectively (Smith *et al.*, 2007). Despite the equivalent age of the upper slide in the core and the MRE

timing along the Fallen Leaf section, we cannot verify that the thin slide imaged above the MRE in Figure 17 correlates with the slide in the core because their relationship is speculative. Nevertheless, using this slide as a marker bed provides a minimum sedimentation rate for this area of ~0.1 mm/yr.

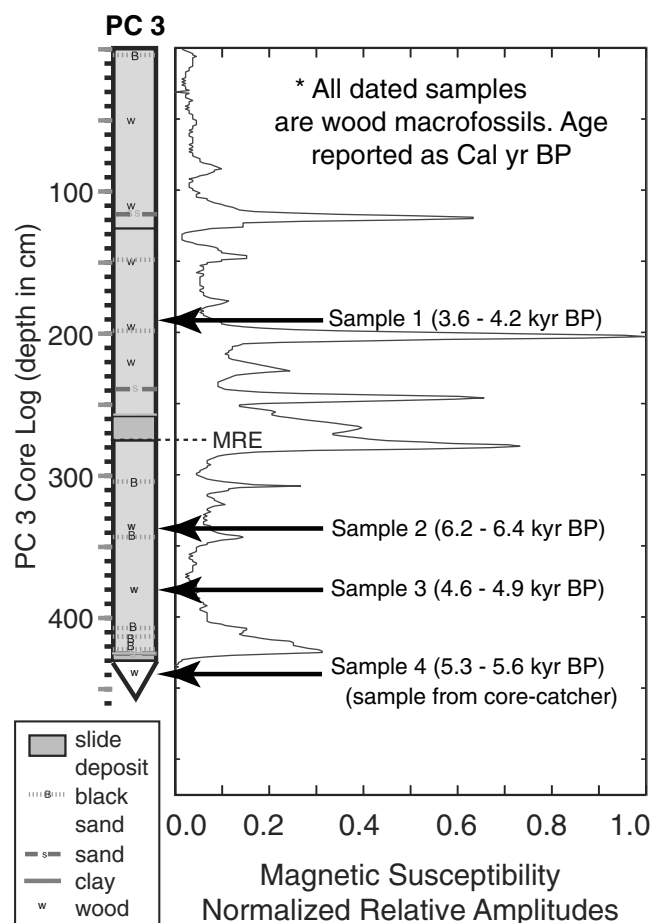


Figure 12. Piston core PC3 lithology and magnetic susceptibility logs. Each of the lithological layers logged can be correlated between all cores except PC5 (Fig. 4). The slide layer, consisting of highly disturbed sand, silt, and clay mixed with several twigs and organics, directly overlies the MRE horizon. Four radiocarbon samples (black arrows; Table 1) were dated to constrain the timing of the MRE. Sample 4, a pine needle, was taken from the core catcher and may have been slightly deeper than 4.3 m due to overpenetration.

The MRE horizon nearest the core in Figure 17 is at ~ 1.4 m depth, resulting in an age of ~ 10 k.y. Sedimentation rates may be expected to increase closer to the basin margins, thus reducing the MRE age estimate. Elsewhere in Lake Tahoe sedimentation rates in the upper 2 m have been estimated as high as ~ 0.4 mm/yr (Smith *et al.*, 2007), which would result in an age for the MRE of ~ 3.5 k.y. B.P.

Offshore Sugar Pine Point the WTDPF offsets a fan delta forming a 10.5 m high scarp observed in both bathymetry and CHIRP data (Fig. 16 and Fig. 18 for the scarp profile). Just north of Sugar Pine Point, the scarp is ~ 90 m tall then disappears at the main run-out area of the MBS debris apron. The Dollar Point section begins at the southern edge of the TCS, where the fault has an ~ 100 m tall scarp and possible slumping and secondary faulting in both the footwall and hanging wall (Fig. 16; Dingler, 2007). The scarp continues along the east edge of the TCS to Dollar Point. The scarps on

either side of the MBS are approximately the same height. The age of the MRE is not constrained on this section.

Discussion

Fallen Leaf Lake Morphology and Stratigraphic Character

FLL has formed through a combination of glacial and tectonic forces. The undulating and hummocky nature of the AB imaged in the northern two-thirds of the lake suggests that a series of recessional and lateral moraines create topography that is being filled with lacustrine sediments (Fig. 4). Formation of the steep slope bounding the basin depocenter may have facilitated glacial erosion along the WTDPF. Any preglacial structure in the bedrock, including an increased fracture density due to faulting, may have created a zone of preferential quarrying along the hanging-wall block on the lee side of glacial flow. The glacial history in the LTB provides rough estimates for the sedimentary history in FLL where it is assumed that Tioga glaciation reworked the inner walls of the moraine-bounded valleys and reset lacustrine sedimentation at ~ 14 ka, when the glaciers recessed (Benson *et al.*, 1998).

The stratigraphy observed in package I (Figs. 6, 8, and 11) reveals that a combination of down-slope and along-slope processes have formed intercalated drift deposits and gravity driven slope deposits. The lenticular beds that thicken toward the center of FLL resemble current controlled deposits that are swept basinward by bottom currents (Driscoll and Laine, 1996). Bathymetric lows along the basin slopes have been filled with coarse-grained beds that onlap the underlying strata. High-amplitude contacts between the lenticular beds and onlapping beds support the notion that coarser-grained down-slope deposits are emplaced on top of finer-grained drift deposits. Contourite drifts are often observed in marine environments along continental margins (Driscoll and Laine, 1996; McGinnis *et al.*, 1997; Faugeres *et al.*, 1999) and in large-scale lacustrine basins (Gilli *et al.*, 2005), but less commonly in small confined basins such as FLL.

The coarse-grained layer above the MRE horizon is observed throughout the southern lake and appears to be a slide deposit. Although disrupted strata beneath the slide (Fig. 10) may be caused by soft sediment deformation during the MRE, the coincidence of coarser-grained (proximal) material in PC1 and the chaotic reflections in Figure 10 suggest the slide source is near the southeastern basin slope (Fig. 9b). The extensive run out (> 1000 m) away from the source region and the absence of coherent internal reflectors indicate the slide deposit was most likely emplaced by a hyperpycnal flow with high velocity. Based on the stratal relationship between the slide and the MRE horizon, it is possible that the slide was triggered by the last major event on the WTDPF. Several smaller slides are identified throughout the basin

Table 1
Radiocarbon Ages Derived from Macrofossil Samples

Location	Lab ^a	Sample Number, Description ^b	Stratigraphic Depth ^c (m)	Lab Identification Number	$\delta^{13}\text{C}$ ^d	Uncalibrated ¹⁴ C Age (yr B.P.)	Calibrated Calendric Age ^e	% Confidence	Rounded Age ^f (k.y. B.P.)
Core 3 (FLL)	UofA	1, wood	1.90	AA76371	-21.9	3580 ± 110	4159–3585 4201–4227	94.1 1.0	3.6–4.2
		2, wood	3.40	AA76375	-26.3	5506 ± 41	4171–4178 6270–6400	0.2 86.5	6.2–6.4
		3, wood	3.83	AA76374	-25.6	4235 ± 44	6214–6242 4785–4869	8.9 45.6	4.6–4.9
Core 4 (FLL)	LLNL	4, pine needle	4.30	128008	-25	4795 ± 45	4620–4765 5458–5607	49.8 89.3	5.3–5.6
		5, fiber	4.10	128009	-25	7995 ± 40	5331–5375 8717–9008	6.1 94.6	8.7–9.0
Core 5 (FLL) Baldwin Beach Tree (LT)	UofA LLNL	6, wood	2.36	AA76376	-26.2	6003 ± 48	8661–8667 6730–6975	0.5 95.4	6.7–7.0
		7, wood	N/A	12628	-25	4705 ± 35	5510–5581 5438–5485	23.1 21.1	5.3–5.6
							5321–5420	51.2	

^aSample analysis was performed at the University of Arizona Accelerator Mass Spectrometry Laboratory (UofA) and the Lawrence Livermore National Laboratory Center for Accelerator Mass Spectrometry (LLNL).

^bAll samples were larger than 5 mg.

^c $\delta^{13}\text{C}$ values equal to -25 were not measured, but are the assumed values according to Stuiver and Polach (1977). All other values were measured.

^dMeasured from top of core.

^eAll dates given as a max–min date range. Raw ¹⁴C ages were calibrated using OxCAL v4.0.5 (Ramsey, 2001) and the IntCal04 atmospheric curve (Reimer *et al.*, 2004). Calibrated ages are reported as % confidence under the 95% probability distribution.

^fRounded ages are reported as a max–min range. Final age ranges are rounded to the nearest 0.1 k.y.

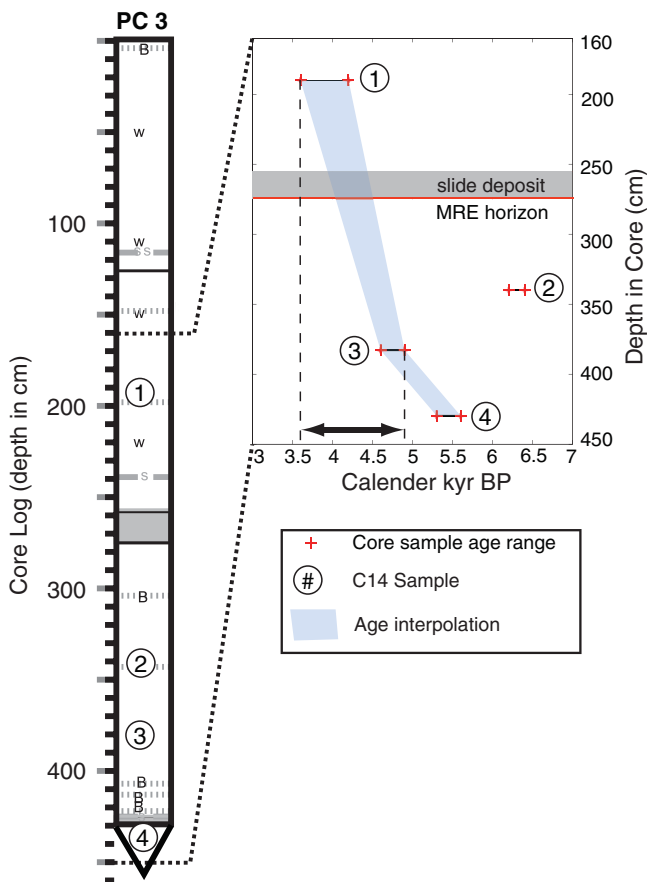


Figure 13. Plot of piston core PC3 sediment depth as a function of age. The age of the MRE was estimated by removing the thickness of the slide then linearly interpolating between samples 1 and 3. Sample 2 appears anomalously old based on its stratigraphic position and was not used in the analysis. The blue region represents the interpolated age range, and the black double-sided arrow indicates the absolute range of ages. The section between samples 1 and 3 is 173 cm and the MRE is at 65 cm after removing the 20 cm thick slide deposit. Interpolating between the upper and lower age ranges results constrains the MRE to between 4.1 and 4.5 k.y. B.P.

based on their acoustic character and range in size from very localized to regional.

Updated Fault Locations

Results from the onshore and offshore fault mapping have improved our understanding of fault locations along the Fallen Leaf section of the WTDPF and add important constraints on the potential rupture length. The southernmost extent of the fault is uncertain as the scarp merges with a steep hillside ~1 km south of Osgood Swamp, but based on the 2–3 m scarp height near this location (Fig. 14), the fault may continue southward for several kilometers. Evidence for faulting offshore Baldwin Beach based solely on CHIRP profiles is ambiguous but, when combined with mapped scarps to the south (meadow scarp) and the lake-floor disruption to the north, suggests that the WTDPF extends offshore near Baldwin Beach. Although the coseismic vertical offset

observed in FLL (Table 2) would be sufficient to drown near-shore vegetation situated east of the fault, the age of the submerged tree offshore Baldwin Beach is slightly older than the age estimate of the MRE. Nonetheless, given the timing of the MRE, it is likely that down-to-the-east motion associated with this event played a role in the ultimate preservation of the submerged trees, and we cannot reject the possibility that an older event submerged the trees but did not rupture through FLL. The mapped extent of the MF in FLL is limited but appears to project northward toward the meadow scarp (Fig. 2). We do not observe offset strata in CHIRP data collected in Emerald Bay, but acoustic penetration was limited toward the mouth of the bay by glacial sediment. North of FLL, the fault may trend towards the eastern shore of Cascade Lake, then across the mouth of Emerald Bay into the Rubicon section. The apparent complexity may be due to inconclusive mapping onshore, a relay zone between sections, or the existence of a broader basin-bounding fault zone, in which multiple faults accommodate extension. The fault's proximity to the steep basin slope creates acoustic interference and hinders our ability to image the sub-bottom using the CHIRP system; therefore, the Rubicon and Dollar Point sections are generally delineated by bathymetric expression.

The minimum estimate for the total length of the combined sections, from the southern terminus of our field mapping to where the Dollar Point section steps onshore in Carnelian Bay, is ~46 km. The fault likely extends onshore at least another 5 km north of Carnelian Bay (Saucedo *et al.*, 2005) and possibly a similar amount south of Osgood Swamp, producing a length of ~55 km. Overall, the length and morphology of the WTDPF is strikingly similar to that of the GF (Fig. 19).

Earthquake Timing, Magnitude, and Slip Rates

The MRE age estimates for the Fallen Leaf (4.1–4.5 k.y. B.P.) and Rubicon (~3–10 k.y. B.P.) sections are in rough agreement and imply the fault may rupture as a single strand. Offset measurements should be considered minimum estimates as the apparent offset (based on constant velocity) is expected to increase in the deeper, more compacted, higher velocity sediments. At FLL, the maximum observed offset of the lacustrine sediments is 3.7 m on the main trace and 1.3 m on the secondary splay, producing a maximum possible offset of 5.0 m. The MF has a 1.6 m of offset but remains poorly understood and may have recorded local deformation following an event on the WTDPF. The ~2 m offset observed along the Rubicon section (Fig. 17) is about half the maximum but within the range of offset values measured beneath FLL (e.g., Fig. 5). The fault observed in Figure 17 may represent a splay off the WTDPF, with a second fault along the base of the slope where acoustic diffractions preclude imaging with the CHIRP system. However, along strike variation in slip is common along normal fault ruptures, in particular near geometric complexities (Witkind *et al.*, 1962; Crone *et al.*, 1987; Ramelli *et al.*, 1999). More

Table 2
 WTDPF Offset Measurements from Chirp Profiles in Fallen Leaf Lake

Profile	MRE Horizon				Depth Horizon				Secondary Splay				Total* (m)
	Footwall (sec)	Hanging wall (sec)	Offset (m)	±(m)	Footwall (sec)	Hanging wall (sec)	Offset (m)	±(m)	Footwall (sec)	Hanging wall (sec)	Offset (m)	±(m)	
Perp01	0.1570	0.1592	1.7	0.2	0.1661	0.1702	3.0	0.2	0.1536	0.1562	1.0	0.2	4.0
Perp02	0.1530	0.1550	0.15	0.2	?	?	?	?	?	?	?	?	
Perp04	0.1589	0.1617	2.0	0.2	0.1780	0.1827	3.5	0.2	0.1575	0.1583	0.6	0.2	4.1
Perp05	0.1577	0.1604	2.0	0.2	0.1733	0.1779	3.5	0.2	0.1574	0.1584	0.8	0.2	4.3
Perp06	0.1604	0.1631	2.0	0.2	0.1736	0.1776	3.0	0.2	?	?	?	?	
Line4	0.1579	0.1611	2.4	0.2	0.1737	0.1780	3.2	0.2	0.1581	0.1598	1.3	0.2	4.5
Line04all [†]	0.1589	0.1626	2.8	0.2	0.1875	0.1923	3.7	0.2	0.1585	0.1597	0.8	0.2	4.5
D3L08 [‡]	0.1577	0.1602	1.9	0.2	0.1779	0.1820	3.1	0.2	0.1602	0.1614	0.9	0.2	3.9
Line03b	0.1568	0.1592	1.7	0.2	0.1679	0.1704	3.0	0.7	?	?	?	?	
Measurements			9				8				6		
Average			2.0				3.3				0.9		
Maximum			2.8				3.7				1.3		
Minimum			1.5				3.0				0.6		

Offset is measured at three places: the MRE horizon, a horizon at greater than 10 m depth, and the MRE horizon of the WTDPF splay. Piercing points on either side of the fault are listed as two-way travel times then converted to depth using a constant 1500 m/sec seismic velocity. All uncertainties are the vertical resolution of the CHIRP source. Offset measurements on Line03b (not shown) have higher uncertainty due to chaotic bedding near the fault.

*The sum of measurements across the depth horizon and the secondary splay.

[†]See Figure 5.

[‡]See Figure 6.

seismic data and coincident coring are required along the Rubicon and Dollar Point sections to evaluate the precise timing and slip during the MRE.

Length and displacement estimates can be used to reconstruct the rupture magnitude for the MRE. The greatest sources of uncertainty in the magnitude calculation arise from measuring the coseismic slip and the total length of rupture, especially in regions with sparse data coverage such as the two northern sections. However, several factors allow us to calculate a worst case scenario magnitude estimate in

which the entire WTDPF ruptured during the MRE: (1) overlap between the MRE timing between the Fallen Leaf and Rubicon sections leads us to believe they could rupture in concert, (2) the Rubicon and Dollar Point sections combined have a linear trend and do not appear to have any major structural discontinuities that would terminate propagation, (3) through-going ruptures are reported on the GF despite a 1.5 km stepover (Ramelli *et al.*, 1999), and (4) ruptures along strike-slip faults suggest the limiting stepover dimension is between 3 and 4 km (Wesnousky, 2006). A range of theoretical moment magnitudes (Hanks and Kanamori, 1979) can be calculated using the minimum slip and minimum rupture length and the maximum slip and maximum rupture length estimates. Assuming all sections rupture concomitantly, we believe the uncertainty in total fault length does not exceed 10 km (20%). However, our maximum slip measurement is along the southernmost 15 km of the fault, which may actually be a better estimate of the average slip because displacement is generally the greatest at fault midpoints (Scholz, 2002). Therefore, we assume slip measured at FLL represents an average value for the entire WTDPF and calculate a theoretical moment magnitude. Using a 4.5 m maximum offset (the combined offset across the WTDPF and secondary splay in FLL), a 55 km fault length and 15 km fault width produces an M 7.33 event. Because we do not understand the nature of the splay and we cannot rule out the possibility for multiple events between the MRE horizon and the deeper offset measurements, a minimum estimate of M 6.81 is calculated using the 2.8 m maximum offset measured across the MRE horizon and a fault length of 15 km for the Fallen Leaf section. However, based on the previous dis-



Figure 14. Photograph of the WTDPF scarp ~500 m south of Osgood Swamp (see Fig. 2 for location). Mapped scarps typically have relaxed profiles with slopes between 20° and 40°, suggesting that significant time has passed since the last surface rupture. White arrow delineates the approximate base of the scarp.

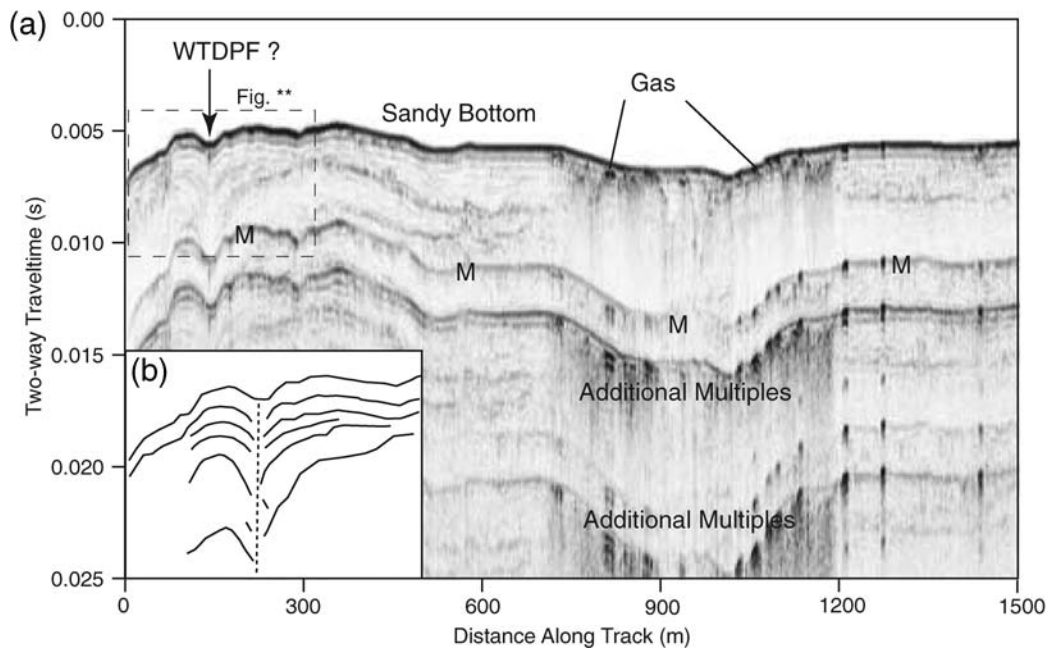


Figure 15. (a) Northwest–southeast oriented profile directly offshore Baldwin Beach (see Fig. 3 for location). Three profiles image a tightly folded syncline that is inferred to be a strand of the WTDPF. Coarse-grained sandy sediments and shallow water multiples limit penetration to ~4 m below the lake floor. There is no penetration beneath the first multiple (M). (b) Interpreted structure within the dashed box.

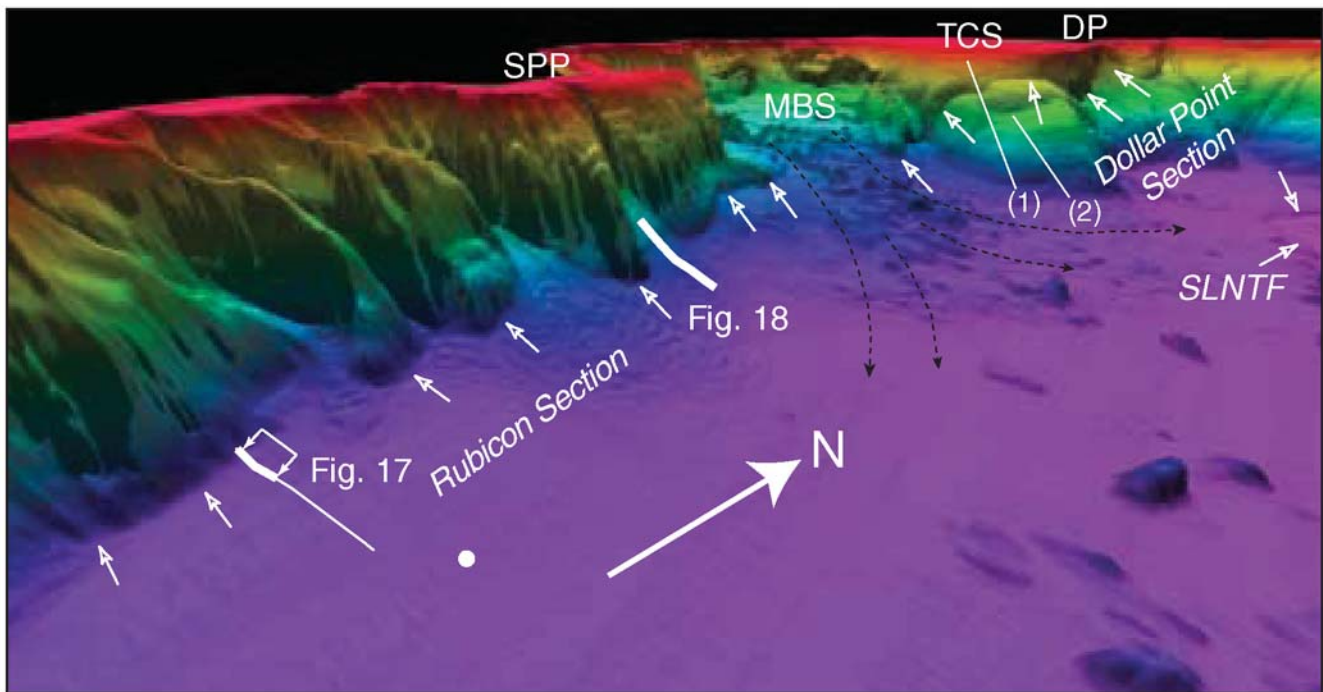


Figure 16. Three-dimensional rendering of Lake Tahoe bathymetry looking northwest along the Rubicon and Dollar Point sections of the WTDPF. Small, open arrows point to fault locations and observed lake-floor scarps; thin black arrows are the approximate transport direction of the MBS debris flow and fan systems. (1) and (2) highlight slumping head scarps and secondary deformation in the hanging wall of the WTDPF. Abbreviations: Sugar Pine Point, SPP; McKinney Bay slide, MBS; Tahoe City shelf, TCS; Dollar Point, DP; West Tahoe–Dollar Point fault, WTDPF; and Stalentine–North Tahoe fault, SLNTF.

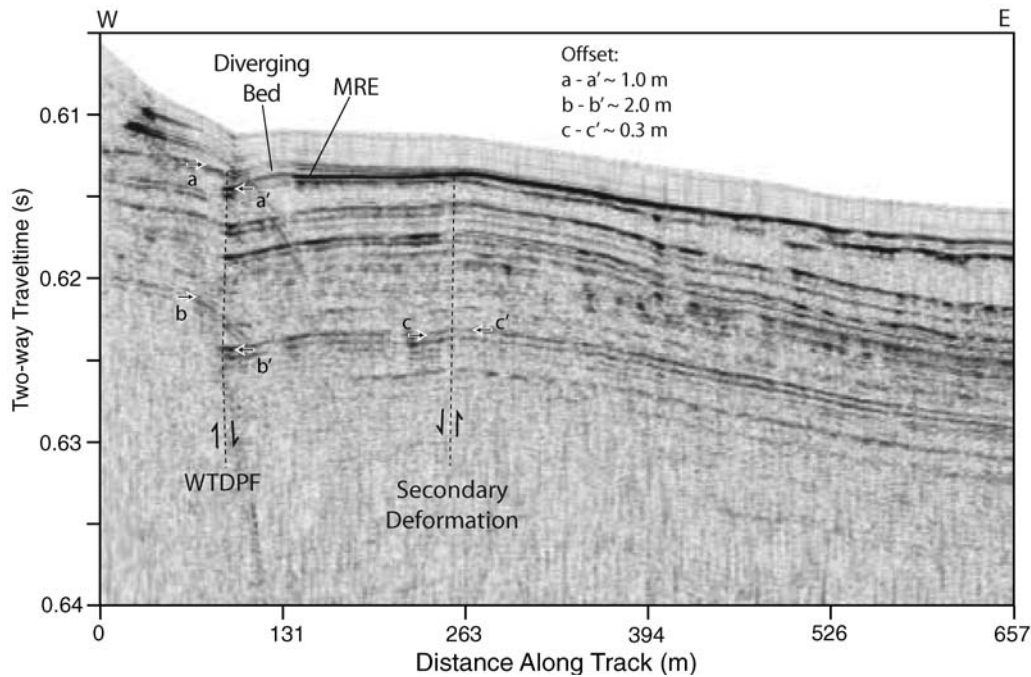


Figure 17. East-west trending profile in Lake Tahoe (see Fig. 3 for location) over the Rubicon section of the WTDPF highlighting offset lake stratigraphy. The MRE horizon is delineated by the sudden change in dip and overlying divergent wedge that thickens into the fault (similar to the deformation observed beneath FLL). Piercing points (white arrows with black interior) measure ~ 1 m down-to-the-east offset across the MRE horizon (aa') and up to ~ 2 m on a deeper horizon (bb'). Note secondary deformation ~ 150 m to the east of the WTDPF, where bedding dip abruptly changes from down-to-the-west to down-to-the-east and layers are slightly folded (> 0.5 m). This may represent secondary deformation associated with either an antithetic fault or hanging-wall collapse. A piston core ~ 800 m to the east of this profile (Smith *et al.*, 2007) provides a rough estimate of the sedimentation rates, and an MRE age between ~ 3.5 and 10 k.y. B.P., which is consistent with the age determined in FLL.

cussion, our best estimate for the magnitude of the MRE employs a fault length of 55 km and an average slip of 3.7 m (the maximum measured across the primary WTDPF splay in FLL), producing an $M 7.27$ event. Using the same parameters

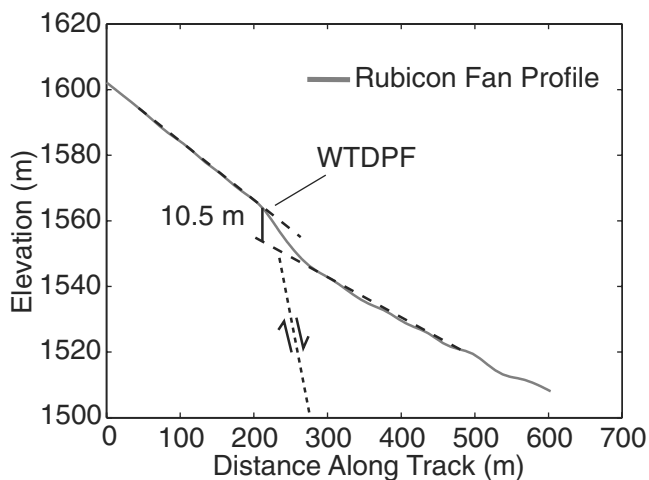


Figure 18. Topographic profile across the Rubicon Fan, offshore Sugar Pine Point (see Fig. 16 for location). A 10.5 m high scarp has formed along the WTDPF and appears to record coseismic deformation since the recession of the Tioga-aged glaciation ~ 14 ka. 10.5 m slip during this period results in an average slip rate between 0.7 and 0.8 mm/yr.

in an empirical magnitude estimate (Wells and Coppersmith, 1994) produces an event between $M 6.89$ and 7.35. In summary, the MRE magnitude estimates are between $M 6.8$ and 7.3, with the latter being the best estimate. This magnitude range is similar to historical large-magnitude earthquakes in the northwestern Basin and Range (Bell *et al.*, 2004; Wells and Coppersmith, 1994), as well as paleoseismic based estimates for the GF (Ramelli *et al.*, 1999).

Slip rates can be calculated in two ways, both of which involve the timing of Tioga glacial retreat. First, if lacustrine sediments in FLL were deposited after the Tioga glacier receded up the valley, we can apply the age of glacial retreat as an upper bound on the age of the tilted strata in Figure 6. We assume the dipping strata were originally deposited horizontally and then subsequently tilted toward the fault during multiple events. Tioga glaciation ceased in the eastern Sierra Nevada between 13 and 14 k.y. B.P. (Phillips *et al.*, 1996; Clark and Gillespie, 1997; Benson *et al.*, 1998), an age range also supported by climate proxies from piston cores collected in Lake Tahoe (Smith *et al.*, 2007); therefore, the 7 ± 2 m offset measured across the dipping beds produces a minimum late-Pleistocene slip rate between 0.4 and 0.7 mm/yr. The seismic velocity used to convert from travel time to depth in the measured section may be as high as 1800 m/sec, which would increase the offset to ~ 10.5 m (upper bound) and the slip rate to ~ 0.8 mm/yr over the last 13 k.y. In the

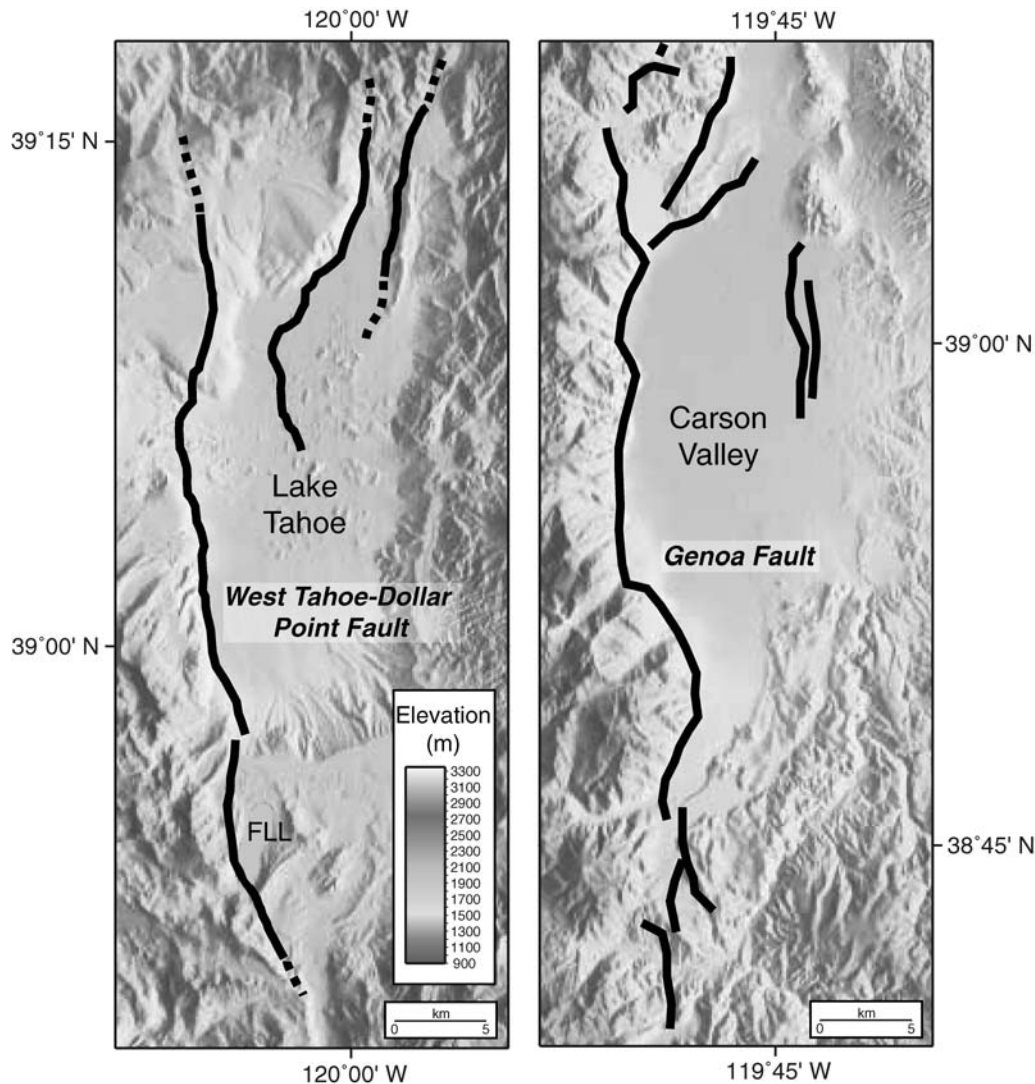


Figure 19. Comparison of the West Tahoe fault and the GF; both faults exhibit similar range front morphology, strike, and length. Together, these faults appear to be accommodating most of the extension (2–3 mm/yr) occurring within the northern Walker Lane at the latitude of Lake Tahoe.

second method, the offset fan surface offshore Sugar Pine Point (Figs. 16 and 18) is presumed to be inactive since the Tioga glacial retreat (Dingler, 2007). The 10.5 m offset (Fig. 18) since 13 k.y. B.P. also produces a maximum vertical slip rate of ~ 0.8 mm/yr. Overall, these data give rise to a vertical displacement rate between 0.4 and 0.8 mm/yr since the end of Tioga glaciation, which is slightly higher than the 0.5 mm/yr minimum slip-rate estimate (over the last ~ 20 ka) reported by Kent *et al.* (2005). An extension rate can be estimated from vertical slip rate assuming simple fault geometry. For a 60° dipping normal fault, the vertical deformation rate is transformed into an extension rate between 0.3 and 0.5 mm/yr. The slip rate along the WTDPF may be higher than estimated because the MRE occurred at 4.1–4.5 k.y. B.P. and, presumably, additional strain has accumulated during the quiescent interval. With a slip rate between 0.4 and 0.8 mm/yr, it is possible that ~ 3 m of elastic strain

has accumulated across the WTDPF. Coseismic slip of 3 m on the WTDPF could generate an $M \geq 7$ event. The GF (Fig. 19) has a vertical deformation rate of 2–3 mm/yr over the last 2 k.y. (Ramelli *et al.*, 1999), which can be converted to a 1.2–1.7 mm/yr extension rate (also assuming 60° dip). The combined extension rates of the GF and the WTDPF are consistent with the 2–3 mm/yr GPS derived extension rates across the Sierra Nevada frontal fault zone (Hammond and Thatcher, 2004, 2007).

Earthquake triggering associated with normal fault earthquakes and resulting static stress changes have been used to explain normal fault event sequences (Nostro *et al.*, 1997); therefore, it is important to compare paleoearthquake records between neighboring faults. Events on the IVF and GF at ~ 500 yr B.P. (Ramelli *et al.*, 1999; Dingler, 2007) suggest a possible relationship in the rupture timing, but the age uncertainty is large and coincident timing could also be re-

lated to dynamic and viscoelastic stress changes. We do not observe any evidence for an event 500 yr B.P. along the Fallen Leaf or Rubicon sections of WTDPF. Although the MRE timing along the SLNTF has not been determined, the proximity (~3 km) of the SLNTF to WTDPF suggests either of these faults may adversely affect stress conditions on the other following a large rupture.

Conclusions

Based on fault length and coseismic slip determined for the MRE, the WTDPF has the potential to generate $M \geq 7.0$ ruptures. The vertical slip rate determined in this study (0.4–0.8 mm/yr) suggests that the WTDPF is amongst the most active normal faults in the western Basin and Range and the northern WLB. With the westward encroachment of extensional faulting since the middle Miocene (Surpluss *et al.*, 2002), the faults in the LTB, may eventually take on higher (2–3 mm/yr) slip rates comparable to that of the GF (Ramelli *et al.*, 1999). Although the northern sections require additional studies, and only one paleoearthquake has been precisely identified on the WTDPF, the new constraints on timing and slip across the WTDPF are important for hazard assessment in the LTB as well as Carson City and Reno, Nevada. Beyond the loss of life and damage associated with ground shaking in large earthquakes, Ichinose *et al.* (2000) predict ~10 m high seiche waves in Lake Tahoe can be generated by 2.83 m (average) of coseismic slip on the WTDPF. If the WTDPF were to produce an $M \geq 7.0$ rupture, the resulting seiche waves would present a significant hazard to lake-front areas.

Data and Resources

The authors collected all seismic CHIRP data and piston cores used in this study. To request data, contact author Daniel Brothers.

Acknowledgments

We would like to acknowledge Captain Brant Allen of the Tahoe Environmental Research Center, John Kleppe, John Rich of the Fallen Leaf Marina, Jenna Hill, Leah Hogarth, and Elizabeth Johnstone for their assistance with fieldwork in Fallen Leaf Lake and Lake Tahoe. We would also like to thank Rich Koehler of the University of Nevada, Reno, for thorough and helpful reviews. This project was funded through U.S. Geological Survey National Hazards Reduction Program (USGS NEHRP) Grant Number 06HQGR0064.

References

- Argus, D. F., and R. G. Gordon (2001). Present tectonic motion across the Coast Ranges and San Andreas fault system in central California, *Geol. Soc. Am. Bull.* **113**, 1580–1592.
- Bacon, C. R. (1983). Eruptive history of Mount Mazama and Crater Lake Caldera, Cascade Range, USA, *J. Volcanol. Geotherm. Res.* **18**, 57–115.
- Bell, J. W., S. J. Caskey, A. R. Ramelli, and L. Guerrieri (2004). Pattern and rates of faulting in the central Nevada seismic belt, and paleoseismic evidence for prior beltlike behavior, *Bull. Seismol. Soc. Am.* **94**, 1229–1254.
- Bennett, R. A., B. P. Wernicke, N. A. Niemi, A. M. Friedrich, and J. L. Davis (2003). Contemporary strain rates in the northern Basin and Range province from GPS data, *Tectonics* **22**, no. 2, 1008, doi 10.1029/2001TC001355.
- Benson, L. V., H. M. May, R. C. Antweiler, T. I. Brinton, M. Kashgarian, J. P. Smoot, and S. P. Lund (1998). Continuous lake-sediment records of glaciation in the Sierra Nevada between 52,600 and 12,500 C-14 yr BP, *Quat. Res.* **50**, 113–127.
- Birkeland, P. W. (1963). Pleistocene volcanism and deformation of the Truckee area, north of Lake Tahoe, California, *Geol. Soc. Am. Bull.* **74**, 1453–1463.
- Bischoff, J. L., and K. Cummins (2001). Wisconsin glaciation of the Sierra Nevada (79,000–15,000 yr BP) as recorded by rock flour in sediments of Owens Lake, California, *Quat. Res.* **55**, 14–24.
- Briggs, R. W., and S. G. Wesnousky (2004). Late Pleistocene fault slip rate, earthquake recurrence, and recency of slip along the Pyramid Lake fault zone, northern Walker Lane, United States, *J. Geophys. Res.-Solid Earth* **109**, B8402, doi 10.1029/2003JB002717
- Briggs, R. W., and S. G. Wesnousky (2005). Late Pleistocene and Holocene paleoearthquake activity of the Olinghouse fault zone, Nevada, *Bull. Seismol. Soc. Am.* **95**, 1301–1313.
- Clark, D. H., and A. R. Gillespie (1997). Timing and significance of late-glacial and Holocene cirque glaciation in the Sierra Nevada, California, *Quat. Int.*, **38–9**, 21–38.
- Crone, A. J., M. N. Machette, M. G. Bonilla, J. J. Lienkaemper, K. L. Pierce, W. E. Scott, and R. C. Bucknam (1987). Surface faulting accompanying the Borah Peak earthquake and segmentation of the Lost River fault, Central Idaho, *Bull. Seismol. Soc. Am.* **77**, 739–770.
- Dingler, J. A. (2007). New geophysical approaches to study neotectonics and associated geohazards, *Ph.D. Thesis*, University of California at San Diego.
- Dixon, T. H., M. Miller, F. Farina, H. Z. Wang, and D. Johnson (2000). Present-day motion of the Sierra Nevada block and some tectonic implications for the Basin and Range province, North American Cordillera, *Tectonics* **19**, 1–24.
- Driscoll, N. W., and E. P. Laine (1996). Abyssal current influence on the southwest Bermuda Rise and surrounding region, *Mar. Geol.* **130**, 231–263.
- Faugeres, J. C., D. A. V. Stow, P. Imbert, and A. Viana (1999). Seismic features diagnostic of contourite drifts, *Mar. Geol.* **162**, 1–38.
- Faulds, J. E., C. D. Henry, and N. H. Hinz (2005). Kinematics of the northern Walker Lane: an incipient transform fault along the Pacific–North American plate boundary, *Geology* **33**, 505–508.
- Gardner, J. V., L. A. Mayer, and J. E. H. Clarke (2000). Morphology and processes in Lake Tahoe (California–Nevada), *Geol. Soc. Am. Bull.* **112**, 736–746.
- Gawthorpe, R. L., I. Sharp, J. R. Underhill, and S. Gupta (1997). Linked sequence stratigraphic and structural evolution of propagating normal faults, *Geology* **25**, 795–798.
- Gilli, A., F. S. Anselmetti, D. Ariztegui, M. Beres, J. A. McKenzie, and V. Markgraf (2005). Seismic stratigraphy, buried beach ridges and contourite drifts: the Late Quaternary history of the closed Lago Cardiel basin, Argentina (49 degrees S), *Sedimentology* **52**, 1–23.
- Hammond, W. C., and W. Thatcher (2004). Contemporary tectonic deformation of the Basin and Range province, western United States: 10 years of observation with the Global Positioning System, *J. Geophys. Res.-Solid Earth* **109**, B08403, doi 10.1029/2003JB002746.
- Hammond, W. C., and W. Thatcher, (2007). Crustal deformation across the Sierra Nevada, northern Walker Lane, Basin and Range transition, western United States measured with GPS, 2000–2004, *J. Geophys. Res.-Solid Earth*, **112**, B05411, doi 10.1029/2006JB004625.
- Hanks, T. C., and H. Kanamori (1979). Moment magnitude scale, *J. Geophys. Res.* **84**, 2348–2350.
- Hardy, S., and K. McClay (1999). Kinematic modelling of extensional fault-propagation folding, *J. Struct. Geol.* **21**, 695–702.

- Hearn, E. H., and E. D. Humphreys (1998). Kinematics of the southern Walker Lane belt and motion of the Sierra Nevada block, California, *J. Geophys. Res.-Solid Earth* **103**, 27033–27049.
- Henry, C. D., and M. E. Perkins (2001). Sierra Nevada-Basin and Range transition near Reno, Nevada: two-stage development at 12 and 3 Ma, *Geology* **29**, 719–722.
- Hyne, N. J., P. Chelmins, D. S. Gorsline, C. R. Goldman, and J. E. Court (1972). Quaternary history of Lake Tahoe, California–Nevada, *Geol. Soc. Am. Bull.* **83**, no. 5, 1435–1448.
- Ichinose, G., J. Anderson, K. Satake, R. Schweickert, and M. Lahren (2000). The potential hazard from tsunami and seiche waves generated by large earthquakes within Lake Tahoe, California–Nevada, *Geophys. Res. Lett.* **27**, no. 8, 1203–1206.
- Ichinose, G. A., J. G. Anderson, K. D. Smith, D. dePolo, R. Anooshehpour, R. A. Schweickert, and M. L. Lahren (1999). The seismotectonics of the 30 October 1998 Incline Village, Nevada earthquakes from regional moment tensor inversion, *Bull. Seismol. Soc. Am.* **70**, 297–305.
- Ichinose, G. A., J. G. Anderson, K. D. Smith, and Y. H. Zeng (2003). Source parameters of eastern California and western Nevada earthquakes from regional moment tensor inversion, *Bull. Seismol. Soc. Am.* **93**, 61–84.
- Kent, G. M., J. M. Babcock, N. W. Driscoll, A. J. Harding, J. A. Dingler, G. G. Seitz, J. V. Gardner, L. A. Mayer, C. R. Goldman, A. C. Heyvaert, R. C. Richards, R. Karlin, C. W. Morgan, P. T. Gayes, and L. A. Owen (2005). 60 k.y. record of extension across the western boundary of the Basin and Range province: estimate of slip rates from offset shoreline terraces and a catastrophic slide beneath Lake Tahoe, *Geology* **33**, 365–368.
- Lindstrom, S. G. (1990). Submerged tree stumps as indicators of mid-Holocene aridity in the Lake Tahoe region, *J. Calif. Gt. Basin Anthropol.* **12**, 146–157.
- McGinnis, J. P., D. E. Hayes, and N. W. Driscoll (1997). Sedimentary processes across the continental rise of the southern Antarctic Peninsula, *Mar. Geol.* **141**, 91–109.
- Nostro, C., M. Cocco, and M. E. Belardinelli (1997). Static stress changes in extensional regimes: an application to southern Apennines (Italy), *Bull. Seismol. Soc. Am.* **87**, 234–248.
- Oldow, J. S. (2003). Active transtensional boundary zone between the western Great Basin and Sierra Nevada block, western US cordillera, *Geology* **31**, 1033–1036.
- Phillips, F. M., M. G. Zreda, L. V. Benson, M. A. Plummer, D. Elmore, and P. Sharma (1996). Chronology for fluctuations in late Pleistocene Sierra Nevada glaciers and lakes, *Science* **274**, 749–751.
- Ramelli, A. R., J. W. Bell, C. M. dePolo, and J. C. Yount (1999). Large-magnitude, late Holocene earthquakes on the Genoa fault, west-central Nevada and eastern California, *Bull. Seismol. Soc. Am.* **89**, 1458–1472.
- Ramsey, C. B. (1995). Radiocarbon calibration and analysis of stratigraphy: the OxCal program, *Radiocarbon* **37**, 425–430.
- Ramsey, C. B. (2001). Development of the radiocarbon calibration program, *Radiocarbon* **43**, no. 2A, 355–363.
- Reimer, P. J., M. G. L. Baillie, E. Bard, A. Bayliss, J. W. Beck, C. J. H. Bertrand, P. G. Blackwell, C. E. Buck, G. S. Burr, K. B. Cutler, P. E. Damon, R. L. Edwards, R. G. Fairbanks, M. Friedrich, T. P. Guilderson, A. G. Hogg, K. A. Hughen, B. Kromer, G. McCormac, S. Manning, C. B. Ramsey, R. W. Reimer, S. Remmele, J. R. Southon, M. Stuiver, S. Talamo, F. W. Taylor, J. van der Plicht, and C. E. Weyhenmeyer (2004). IntCal04 terrestrial radiocarbon age calibration, 0–26 cal kyr BP, *Radiocarbon* **46**, 1029–1058.
- Sarna-Wojkicki, A. M., K. R. Lajoie, C. E. Meyer, D. P. Adam, and H. J. Rieck (1991). Tephrochronologic correlation of upper Neogene sediments along the Pacific margin, conterminous United States, in *Quaternary Non-Glacial Geology: Conterminous United States*, in The Decade of North American Geology, R. B. Morrison (Editor), Geological Society of America, Boulder, Colorado, Vol. **K-2**, 117–140.
- Saucedo, G. J., J. D. Little, S. E. Watkins, J. R. Davis, M. T. Mascorro, V. D. Walker, and E. W. Ford (2005). Geologic map of the Lake Tahoe Basin, California and Nevada, California Geological Survey, scale 1:100,000.
- Scholz, C. H. (2002). The mechanics of earthquakes and faulting, Second Ed., Cambridge U. Press, Cambridge, UK, 439 pp..
- Schweickert, R. A., M. M. Lahren, K. D. Smith, and R. Karlin (1999). Preliminary fault map of the Lake Tahoe Basin, California and Nevada, *Seism. Res. Lett.* **70**, 306–312.
- Smith, K. D., D. von Seggern, G. Blewitt, L. Preston, J. G. Anderson, B. P. Wernicke, and J. L. Davis (2004). Evidence for deep magma injection beneath Lake Tahoe, Nevada–California, *Science* **305**, 1277–1280.
- Smith, S. B., R. Karlin, G. G. Seitz, and G. M. Kent (2007). Clastic sedimentation in Lake Tahoe as a record for submarine landsliding and seismic shaking (Abstract OS33A-1000), *Eos. Trans. AGU* **88**, OS33A-1000.
- Stewart, J. H. (1988). Tectonics of the Walker Lane belt, western Great Basin–Mesozoic and Cenozoic deformation in a zone of shear, in *Metamorphism and Crustal Evolution of the Western United States*, W. G. Ernst (Editor), Vol. **VII**, Prentice-Hall, Englewood Cliffs, New Jersey, 683–713.
- Stuiver, M., and H. A. Polach (1977). Reporting of C^{14} data, *Radiocarbon* **19**, no. 3, 355–363.
- Surpless, B. E., D. F. Stockli, T. A. Dumitru, and E. L. Miller. (2002). Two-phase westward encroachment of Basin and Range extension into the northern Sierra Nevada, *Tectonics* **21**, no. 1, doi 10.1029/2000TC001257.
- Svarc, J. L., J. C. Savage, W. H. Prescott, and A. R. Ramelli (2002). Strain accumulation and rotation in western Nevada, 1993–2000, *J. Geophys. Res.-Solid Earth* **107**, no. B5, doi 10.1029/2001JB000579.
- Unruh, J., J. Humphrey, and A. Barron (2003). Transtensional model for the Sierra Nevada frontal fault system, eastern California, *Geology* **31**, 327–330.
- Wells, D. L., and K. J. Coppersmith (1994). New empirical relationships among magnitude, rupture length, rupture width, rupture area, and surface displacement, *Bull. Seismol. Soc. Am.* **84**, 974–1002.
- Wesnousky, S. G. (2006). Predicting the endpoints of earthquake ruptures, *Nature* **444**, 358–360.
- Witkind, I. J., W. B. Myers, J. B. Hadley, W. Hamilton, and G. D. Fraser (1962). Geologic features of the earthquake at Hebgen Lake, Montana, August 17, 1959, *Bull. Seismol. Soc. Am.* **52**, 163–180.
- Scripps Institution of Oceanography
University of California, San Diego
9500 Gilman Drive
La Jolla, California 92093-0225
dbrother@ucsd.edu
(D.S.B., G.M.K., N.W.D., J.A.D., A.J.H., J.M.B.)
- Department of Geological Sciences/172
University of Nevada, Reno
1664 N. Virginia St.
Reno, Nevada 89557-0138
(S.B.S., R.K.)
- Department of Geological Sciences
San Diego State University
5500 Campanile Drive
San Diego, California 92182
(G.G.S.)